



An Optimal Synchronization Control Method of PLL Utilizing Adaptive Dynamic Programming to Synchronize Inverter-Based Resources With Unbalanced, Low-Inertia, and Very Weak Grids

Davari, Masoud; Gao, Weinan; Aghazadeh, Amir; Blaabjerg, Frede; Lewis, Frank L.

Published in:
IEEE Transactions on Automation Science and Engineering

DOI (link to publication from Publisher):
[10.1109/TASE.2023.3329479](https://doi.org/10.1109/TASE.2023.3329479)

Publication date:
2024

Document Version
Publisher's PDF, also known as Version of record

[Link to publication from Aalborg University](#)

Citation for published version (APA):
Davari, M., Gao, W., Aghazadeh, A., Blaabjerg, F., & Lewis, F. L. (2024). An Optimal Synchronization Control Method of PLL Utilizing Adaptive Dynamic Programming to Synchronize Inverter-Based Resources With Unbalanced, Low-Inertia, and Very Weak Grids. *IEEE Transactions on Automation Science and Engineering*, 22, 1-19. Article 10478108. <https://doi.org/10.1109/TASE.2023.3329479>

General rights

Copyright and moral rights for the publications made accessible in the public portal are retained by the authors and/or other copyright owners and it is a condition of accessing publications that users recognise and abide by the legal requirements associated with these rights.

- Users may download and print one copy of any publication from the public portal for the purpose of private study or research.
- You may not further distribute the material or use it for any profit-making activity or commercial gain
- You may freely distribute the URL identifying the publication in the public portal -

Take down policy

If you believe that this document breaches copyright please contact us at vbn@aub.aau.dk providing details, and we will remove access to the work immediately and investigate your claim.

An Optimal Synchronization Control Method of PLL Utilizing Adaptive Dynamic Programming to Synchronize Inverter-Based Resources With Unbalanced, Low-Inertia, and Very Weak Grids

Masoud Davari¹, Senior Member, IEEE, Weinan Gao², Senior Member, IEEE,
Amir Aghazadeh³, Graduate Student Member, IEEE, Frede Blaabjerg⁴, Fellow, IEEE,
and Frank L. Lewis⁵, Life Fellow, IEEE

Abstract—When it comes to integrating inverter-based resources (IBRs) into modern grids with varying characteristics like unbalanced systems, low-inertia networks, or very weak grids, synthesizing the synchronization control method (SCM) of the IBR's phase-locked loop can be a challenging task. This paper provides a unique solution to enhance the three-phase IBR's SCM using the adaptive dynamic programming (ADP) method based on reinforcement learning. By making the SCM more intelligent and self-learning, IBRs can be easily integrated into diverse grids. To this end, this article investigates the synchronization process's detailed dynamics, including all incorporating disturbances and parameters required for the first step in designing the ADP method. Afterward, this research synthesizes an optimal controller using an ADP method. It is a data-driven and practically sound approach to the problem under investigation. The new methodology is based on the adaptive

optimal control employing measurement feedback to control the output regulation problem of uncertain synchronization process dynamics via the internal model principle. The proposed SCM design deploys an ADP learning methodology to tackle uncertain parameters and unknown disturbance signals to synchronize IBRs during transients, thereby enhancing IBRs' synchronization in challenging conditions of modern power systems with unbalanced, low-inertia, and very weak grids. For comparison purposes, this paper applies a robust controller based on the well-established μ synthesis approach (benefiting from the well-known D - K iteration process). Comparative simulations are performed; experiments are conducted to reveal the effectiveness and practicality of the ADP-based optimal SCM proposed in this paper.

Note to Practitioners—As different nations strive to combat global warming and accelerate decarbonization, power and energy systems are undergoing a significant shift. Inverter-based resources are being used as an essential component to achieve these goals. However, studies have revealed that designing synchronization control methods of the inverter-based resources' phase-locked loop in unbalanced, low-inertia, and very weak grids is challenging due to the need for accurate dynamic models and other factors. This study revisits the synchronization process's detailed dynamics. It also proposes a novel adaptive dynamic programming strategy using intelligent self-learning approaches to the synchronization control method associated with inverter-based resources. This method utilizes an optimal control to synthesize the adaptive dynamic programming control strategy for the inverter-based resources' synchronization process. Besides, it employs measurement feedback to control the output regulation problem of uncertain dynamics of inverter-based resources' synchronization process via the internal model principle. As a result, this paper makes this process data-driven. It utilizes a learning methodology using adaptive dynamic programming to address uncertain parameters and unknown disturbance signals associated with the dynamics derived and formulated for the problem under investigation. Thus, the proposed method applies to controlling inverter-based resources' synchronization process even in cases with slow parameter variations caused by different factors. It can compensate for all functional disturbance signals affecting the dynamics of the systems. In fact, unlike traditional methods that need an exact dynamic model of the inverter-based resources' synchronization process to design and tune the controller to achieve a proper transient response, the proposed control system trains itself and does so. This study's simulations and experiments reveal that the above points give the proposed approach a competitive edge over the existing methodologies.

Manuscript received 12 February 2023; revised 7 August 2023; accepted 13 October 2023. This article was recommended for publication by Associate Editor M. Robba and Editor Q. Zhao upon evaluation of the reviewers' comments. The work of Masoud Davari was supported in part by the U.S.-Denmark INNOVATOR Program between Georgia Southern University, Statesboro, GA, USA, and Aalborg University, Aalborg, Denmark, funded by the International Research Experiences for Students (IRES) Program in the Office of International Science and Engineering (OISE), U.S. National Science Foundation (U.S. NSF) under U.S. NSF OISE-IRES Award 2152905; in part by the U.S. NSF Energy, Power, Control and Networks (EPCN) Program within the Division of Electrical, Communications and Cyber Systems (ECCS) under ECCS-EPCN Award 1902787 and ECCS-EPCN Award 1808279; in part by the dSPACE Company, Verivolt Company, the Professional Development Part of Masoud Davari's Discovery & Innovation Award from the 2020–2021 University Awards of Excellence at Georgia Southern University; and in part by the 2022 Impact Area Accelerator Grant funded by Georgia Southern University—where all experiments to test the effectiveness of the proposed method were conducted. The work of Weinan Gao was supported in part by the National Natural Science Foundation of China under Grant 62373090. (Corresponding authors: Weinan Gao; Masoud Davari.)

Masoud Davari is with the Department of Electrical and Computer Engineering, Georgia Southern University (Statesboro Campus), Statesboro, GA 30460 USA (e-mail: mdavari@georgiasouthern.edu; davari@ualberta.ca).

Weinan Gao is with the State Key Laboratory of Synthetical Automation for Process Industries, Northeastern University, Shenyang 110819, China (e-mail: gaojn@mail.neu.edu.cn).

Amir Aghazadeh is with the School of Electronic and Electrical Engineering, University of Leeds, LS2 9JT Leeds, U.K. (e-mail: elaagh@leeds.ac.uk).

Frede Blaabjerg is with the AAU Energy, Aalborg University, 9220 Aalborg, Denmark (e-mail: fbl@energy.aau.dk).

Frank L. Lewis is with the UTA Research Institute, The University of Texas at Arlington, Fort Worth, TX 76118 USA (e-mail: lewis@uta.edu).

Color versions of one or more figures in this article are available at <https://doi.org/10.1109/TASE.2023.3329479>.

Digital Object Identifier 10.1109/TASE.2023.3329479

Index Terms—Adaptive dynamic programming (ADP), D - K iteration process, grid synchronization, inverter-based resources (IBRs), μ -synthesis-based robust controller, phase-locked loop (PLL), reinforcement learning, synchronization control method (SCM), voltage-source (or voltage-sourced) converter.

NOMENCLATURE

A. Variables of the Grid-Connected IBR

H	Inertia constant.
\vec{i}	Space-phasor of the ac-side filtered current with the amplitude and phase of i_{dq} and $(\rho_{PLL} + \delta_1)$ in the dq -frame, respectively.
\vec{i}_{Grid}	Space-phasor of the grid current.
\vec{i}_{Load}	Space-phasor of the PCC load current with the amplitude and phase of $i_{Load-dq}$ and $(\rho_{PLL} + \delta_3)$ in the dq -frame, respectively.
J	Moment of inertia.
L_{f-AC}	Inductance of the of the IBR's ac-side filter.
L_{Grid}	Inductance of the ac-side grid's Thevenin equivalent.
L_{GWQ}	Grid-weakness-quantifying parameter based on grid inductance and IBR's ac-side filter inductance.
ω_{Grid}	Grid angular frequency.
ω_{PLL}	Angular frequency generated by the synchronization process.
R_{f-AC}	Resistance of the of the IBR's ac-side filter.
R_{Grid}	Resistance of the ac-side grid's Thevenin equivalent.
ρ_{Grid}	Grid angle.
ρ_{PLL}	Angle generated by the synchronization process.
SCCR	short-circuit capacity ratio.
V_{DC}	IBR's dc voltage filtered by the dc-side filter.
\vec{v}_{PCC}	Space-phasor of the PCC voltage with the amplitude and phase of v_{PCC-dq} and ρ_{PLL} in the dq -frame, respectively.
\vec{v}_t	Space-phasor of the IBR's ac-side boundary (terminal) voltage with the amplitude and phase of v_{t-dq} and $(\rho_{PLL} + \delta_2)$ in the dq -frame, respectively.
\vec{v}_{th}	Space-phasor of the grid-side Thevenin voltage with the amplitude and phase of v_{th-dq} and $(\omega_{Grid}t + \theta_0)$ in the dq -frame, respectively.

B. Variables of the ADP-Based Control

ϵ	Stopping criterion of Algorithm 1.
j	Learning iteration.
K^*	Optimal feedback control gain.
K_j	State-feedback control gain learned at iteration j .
P_j	Value of the learned P at iteration j .

I. INTRODUCTION

INVERTER-BASED resources (IBRs) are enabling power electronic devices to integrate renewables and battery systems into all sections of current and future power and energy systems [1], [2], [3], [4], [5], [6], [7], [8], [9], [10], [11], [12]. In different studies, scholars have shown that current-controlled, grid-connected three-phase IBRs (hereinafter called grid-connected IBRs), while highly beneficial to modern

microgrids and commercial power systems, may encounter issues related to synchronization in unbalanced, low-inertia, and very weak grids. These problems can lead to instability and subpar transient performance, ultimately hindering their effectiveness (see [13], [14], [15], [16] and references therein).

In order to solve synchronization challenges, new kinds of phase-locked loops (PLLs) based on the synchronous reference frame (SRF) have been proposed. They deploy filters in different parts of the PLL structure (see [17] for details about PLL structures). Still, altering the structure of the synchronization process, e.g., PLL, via adding filters in various sections is *not* within the scope of this article, as this matter cannot drastically help address the challenges considered in this article, i.e., optimal design, stability, and transient performance. Instead, the synchronization control method (SCM) of the synchronization process of “three-phase” IBRs is solely covered in this research. Indeed, the synchronization process dynamics, induced and governed by its controller, are among the game changers in the issues associated with IBR's integration into different grids. In this direction, a brief review of the state-of-the-art research conducted is conducted below. Hereinafter, the word “SCM” refers to the “three-phase” IBR's SCM.

A. Brief Literature Review of Recent Developments in SCM

Different scholars have studied various types of SCMs. Some studies have not considered weak-grid conditions during the control design process, while some have taken care of them when synthesizing the controller (see [17] and references therein). Also, for grid integration studies considering grid stiffness, an index known as short-circuit ratio (SCR) [or equivalently short-circuit capacity ratio (SCCR)] is introduced. The SCCR index is defined as the ratio of the grid short-circuit capacity at the point of common coupling (PCC) to the rated power of IBR [14]. It should be mentioned that in weak and very weak conditions (i.e., low values of SCCR close to 1), SCM enormously creates instabilities for IBRs. It is because—in this condition—SCM significantly increases the undesirable interaction between itself and grid impedance [14].

Since the standard vector control strategy is among the controllers frequently utilized in the power converter industry, a vast range of controllers has been investigated. They have been deployed to improve the performance of vector-controlled IBRs integrated into a weak or very weak grid. An improved current control strategy with additional voltage angle and magnitude compensations has been suggested in [18]. A robust vector control of the IBRs integrated into weak grids considering synchronization process dynamics has been addressed in [14] and [19]. As the SCM effect has not been considered in conventional methods to tune the parameters of current controllers [i.e., proportional-integral (PI) controllers] of an LCL -type grid-connected IBR, new design guidance has been presented in order to reduce the negative impact of SCM on the current control in [20]. A simple small-signal disturbance compensation control method, which can be visualized, has been employed to mitigate the problem described above

without modifying the parameters of the synchronization process in [21], requiring an accurate synchronization process's dynamic model.

Numerous studies have examined ways to mitigate instability problems during the synchronization process by adjusting parameters and creating controllers for the vector control strategy. For example, the authors in [22] and [23] have explored different methods, including reducing the SCM gains. Although these methods effectively reduce SCM's negative impact, converter performance constraints limit their functioning [24]. Similar to [20], a new controller design has been addressed in [25]. However, instead of the current controller parameter adjustment, the parameters of SCM have been tuned—thus requiring the system dynamics. In order to integrate fast-switching IBRs (based on the silicon carbide technology) into weak grids, a new control design has been proposed by taking into account the fact that the bandwidth of the synchronization process might not linearly increase with an increase in that of the current loop [26]. In [26], the parameters of the synchronization process have been tuned by considering the coupling between the synchronization process and the current loop; nevertheless, the current controllers have been adjusted independently.

An impedance-compensated SRF synchronization process with phase angle correction has been investigated in [27]. This method compensates for the angle of the synchronization process according to the impedance which is either measured or estimated. As detailed in the methodologies introduced in [20], [22], [23], [24], [25], [26], [27], they fully or partially require the model of the synchronization process dynamics.

Scholars have also investigated a symmetrical structure for the synchronization process. It has been proposed in order to enhance the stability of converter integration into weak grids and remove the frequency-coupling effect [28]. The approach SCM introduced in [28] has simplified the whole system and made it a simple single-input, single-output system facilitating stability analysis. Although the methods stated earlier effectively enable grid-connected IBRs and inverters to be integrated into weak grids, their designs are still “model-based” according to the proposed methodologies.

The authors of [29] have introduced an SCM based on repetitive learning. While SCM enables grid-connected IBRs to integrate into a weak grid with distorted voltages, it has yet to be optimally synthesized—as no optimal control design constraints have been involved in the design process. An enhanced synchronization process that is able to reject disturbances with a fast transient response has been proposed in [30]. Albeit this synchronization process shows promising results in different cases and its performance has been examined via simulations, it still requires the dynamic system model; additionally, it is not based on any optimal control design. In order to address the latter, the authors of [31] have proposed one of the latest optimal controllers based on the linear quadratic regulator (LQR) approach. Yet, the LQR-based methodology introduced therein is based on the precise dynamic model of PLL. As a result, any uncertainty in the dynamic model will eventually result in a *non-optimal* response.

According to the literature review of SCMs conducted and detailed above, having the SCM dynamic model is necessary. It includes the operating point of the IBR, PCC load conditions, and grid characteristics, i.e., grid impedance (type and value) and grid inertia. The last one matters as low-inertia IBRs are integrated into the fully integrated power and energy systems of modern microgrids more and more. Additionally, those parameters and factors are inherently uncertain and sometimes almost *unmeasurable*—meaning the optimal operation and control of the synchronization process may not always be achievable.

Furthermore, simple adaptive control methods cannot be the most suitable option to tackle all the earlier issues simultaneously since the rate of change in the factors mentioned above is genuinely different. Another reason is that those characteristics may not be easily measured or estimated fast enough to be incorporated into the control. For example, operating point changes abruptly happen to meet the load demand, and grid impedance type/value is almost unmeasurable or changeable (because of line maintenance, etc.). Indeed, no existing SCM is independent of the IBR's system model and can train itself by data without any information on the system model to have the desired performance. Last but not least, all the studies cited above may lose synchronization during the transients caused by the low moment of inertia in grids dominated by IBRs.

B. Proposed Contributions

The reinforcement learning algorithms derived from machine learning in the field of artificial intelligence have become popular in various disciplines, including power electronics. These algorithms are useful in enabling engineers to analyze and control power electronic systems more efficiently—much like how humans learn and reason. Consequently, some data-driven control approaches based on reinforcement learning are required for SCM. Simultaneously, the optimality of the control design should be considered. To this end, the following are the significant contributions of this article.

- 1) To the best of the authors' knowledge and according to the most recent online literature reviewed above, it proposes a novel adaptive dynamic programming (ADP, also known as approximate dynamic programming) algorithm to equip SCM with reinforcement learning for the first time. The ADP-based control methodology—a data-driven yet practically sound approach—is currently utilized in many applications, e.g., power engineering [2], [32], [33], [34].
- 2) It proposes a dynamic model of the conventional synchronization process employed in different IBR applications. The proposed model incorporates all of the factors impacting the synchronization process dynamics. To this end, precisely identifying all the parameters and frequency contents of the relevant disturbance signals is crucial to analyzing the required control theories in this research.
- 3) It introduces an optimal control based on the ADP method for SCM without precise information on the

dynamic model, thereby providing a way to solve the adaptive and optimal control problem for an SCM in a successive iterative fashion. Therefore, it is unnecessary to have all the parameters of the dynamic model of the synchronization process known or measurable.

- 4) It proposes a design approach based on the adaptive optimal control to solve a disturbance rejection problem for the uncertain dynamics of the synchronization process via the internal model principle. In this regard, it combines ADP with the internal model principle for SCM to tackle all grid conditions.
- 5) It presents the SCM design procedure with uncertain parameters and unknown disturbance signals. This consideration matches the proposed SCM problem formulation to the practical aspect of a synchronization process. In this regard, by reinforcement learning, the proposed ADP learning strategy deploys a value iteration independent of an initial stabilizing control policy.

This article's structure is as follows. Section II mathematically models the detailed dynamics of the synchronization process, considering all parameters and impactful disturbances for all cases. It is worth mentioning that the synchronization process dynamics are required in the methodology detailed in Section III, as it is necessary to know how to design a model-based optimal controller first. Section III elaborates on the proposed controller's principles, considering what an SCM requires. Section IV demonstrates the simulation results (generated by the proposed ADP-based control), comparative outcomes (produced by the robust controller based on the famous technique of μ synthesis using D - K iteration process), and experimental outcomes. Finally, Section V concludes the contributions.

II. SYSTEM UNDER STUDY

In order to synthesize the data-driven SCM proposed in this paper, the first step is to design a model-based optimal controller. To this end, a *detailed* dynamic model of the synchronization process is necessary. In this regard, all parameters impacting the IBR's synchronization process—including the grid impedance; the ac-side filter dynamics; and the operating point linked to active power and reactive power, the angle of the synchronization process, and that of the actual grid—must be considered. This matter has not been thoroughly studied enough in the literature as current scholarly studies have not brought all factors into one comprehensive enough dynamic model.

Consequently, this section elaborates on the detailed dynamics of the synchronization process. In this regard, all impactful parameters and signals affecting the dynamic model are extracted. To this end, Subsection II-A details the synchronization process dynamics, and Subsection II-B provides the model validation.

A. Detailed Dynamic Model

Fig. 1 shows the detailed structure of a grid-connected three-phase IBR employed in modern grids. The following equations

describe its dynamics in the space-phasor domain.

$$\begin{cases} \vec{v}_{\text{PCC}} = L_{\text{Grid}} \frac{d\vec{i}_{\text{Grid}}}{dt} + R_{\text{Grid}} \vec{i}_{\text{Grid}} + \vec{v}_{\text{th}} \\ \frac{d\vec{i}}{dt} = -\frac{R_{f\text{-AC}}}{L_{f\text{-AC}}} \vec{i} + \frac{1}{L_{f\text{-AC}}} \vec{v}_t - \frac{1}{L_{f\text{-AC}}} \vec{v}_{\text{PCC}} \\ \vec{i}_{\text{Grid}} = \vec{i} - \vec{i}_{\text{Load}}, \end{cases} \quad (1)$$

where \vec{v}_{PCC} is the space-phasor of the PCC voltage representing $v_{\text{PCC-a}}$, $v_{\text{PCC-b}}$, and $v_{\text{PCC-c}}$; L_{Grid} and R_{Grid} (making the impedance Z_{Grid}) are the inductance and resistance of the ac-side grid's Thevenin equivalent, respectively; $L_{f\text{-AC}}$ and $R_{f\text{-AC}}$ are the inductance and resistance of the IBR's ac-side filter, respectively; \vec{i}_{Grid} is the space-phasor of the grid current representing $i_{\text{Grid-a}}$, $i_{\text{Grid-b}}$, and $i_{\text{Grid-c}}$; \vec{i} is the space-phasor of the ac-side filtered current representing i_a , i_b , and i_c ; \vec{v}_{th} is the space-phasor of the grid-side Thevenin voltage representing $v_{\text{th-a}}$, $v_{\text{th-b}}$, and $v_{\text{th-c}}$; \vec{v}_t is the space-phasor of the IBR's ac-side boundary (terminal) voltage representing v_{t-a} , v_{t-b} , and v_{t-c} ; and \vec{i}_{Load} is the space-phasor of the PCC load current representing $i_{\text{Load-a}}$, $i_{\text{Load-b}}$, and $i_{\text{Load-c}}$.

All of the parameters and signals expressed in (1) are shown in Fig. 1. It is worth mentioning that the impedances/signals with a prime symbol of "′" in Fig. 1(a) [i.e., in \vec{i}'_{Grid} (for $i'_{\text{Grid-a}}$, $i'_{\text{Grid-b}}$, and $i'_{\text{Grid-c}}$), \vec{v}'_{th} (for $v'_{\text{th-a}}$, $v'_{\text{th-b}}$, and $v'_{\text{th-c}}$), and Z'_{Grid} (for L'_{Grid} and R'_{Grid})] are the related impedances/signals referred to the step-up transformer's grid-side winding. Therefore, \vec{i}_{Grid} (for $i_{\text{Grid-a}}$, $i_{\text{Grid-b}}$, and $i_{\text{Grid-c}}$), \vec{v}_{th} (for $v_{\text{th-a}}$, $v_{\text{th-b}}$, and $v_{\text{th-c}}$), and Z_{Grid} (for L_{Grid} and R_{Grid}) are their counterparts referred to the step-up transformer's converter-side winding.

By substitution, (1) is expressed as

$$\begin{aligned} \vec{v}_{\text{PCC}} = & -\frac{R_{f\text{-AC}} L_{\text{Grid}}}{L_{f\text{-AC}}} \vec{i} + \frac{L_{\text{Grid}}}{L_{f\text{-AC}}} \vec{v}_t - \frac{L_{\text{Grid}}}{L_{f\text{-AC}}} \vec{v}_{\text{PCC}} \\ & - L_{\text{Grid}} \frac{d\vec{i}_{\text{Load}}}{dt} + R_{\text{Grid}} \vec{i} - R_{\text{Grid}} \vec{i}_{\text{Load}} + \vec{v}_{\text{th}}. \end{aligned} \quad (2)$$

If L_{GWQ} is defined as $\frac{L_{\text{Grid}}}{L_{f\text{-AC}}}$ (i.e., $L_{\text{GWQ}} \triangleq \frac{L_{\text{Grid}}}{L_{f\text{-AC}}}$), L_{GWQ} quantifies the grid weakness based on its impedance divided by the ac-side filter inductance and is hereinafter called grid-weakness-quantifying parameter. The grid-weakness-quantifying parameter L_{GWQ} can be regarded as the counterpart parameter of the inertia constant H quantifying the grid inertia. Therefore, (2) becomes

$$\begin{aligned} (1 + L_{\text{GWQ}}) \vec{v}_{\text{PCC}} = & (R_{\text{Grid}} - R_{f\text{-AC}} L_{\text{GWQ}}) \vec{i} - R_{\text{Grid}} \vec{i}_{\text{Load}} \\ & + L_{\text{GWQ}} \vec{v}_t - L_{\text{Grid}} \frac{d\vec{i}_{\text{Load}}}{dt} + \vec{v}_{\text{th}}. \end{aligned} \quad (3)$$

Now, if all of the space-phasors are defined by their counterparts in the dq -frame, one obtains

$$\begin{cases} \vec{v}_{\text{PCC}} = v_{\text{PCC-dq}} e^{j\rho_{\text{PLL}}} \\ \vec{i} = i_{\text{dq}} e^{j(\rho_{\text{PLL}} + \delta_1)} \\ \vec{v}_t = v_{t\text{-dq}} e^{j(\rho_{\text{PLL}} + \delta_2)} \\ \vec{i}_{\text{Load}} = i_{\text{Load-dq}} e^{j(\rho_{\text{PLL}} + \delta_3)} \\ \vec{v}_{\text{th}} = v_{\text{th-dq}} e^{j(\omega_{\text{Grid}} t + \theta_0)}, \end{cases} \quad (4)$$

where $v_{\text{PCC-dq}}$ and ρ_{PLL} represent the amplitude and phase of \vec{v}_{PCC} , respectively; i_{dq} and $(\rho_{\text{PLL}} + \delta_1)$ represent the amplitude

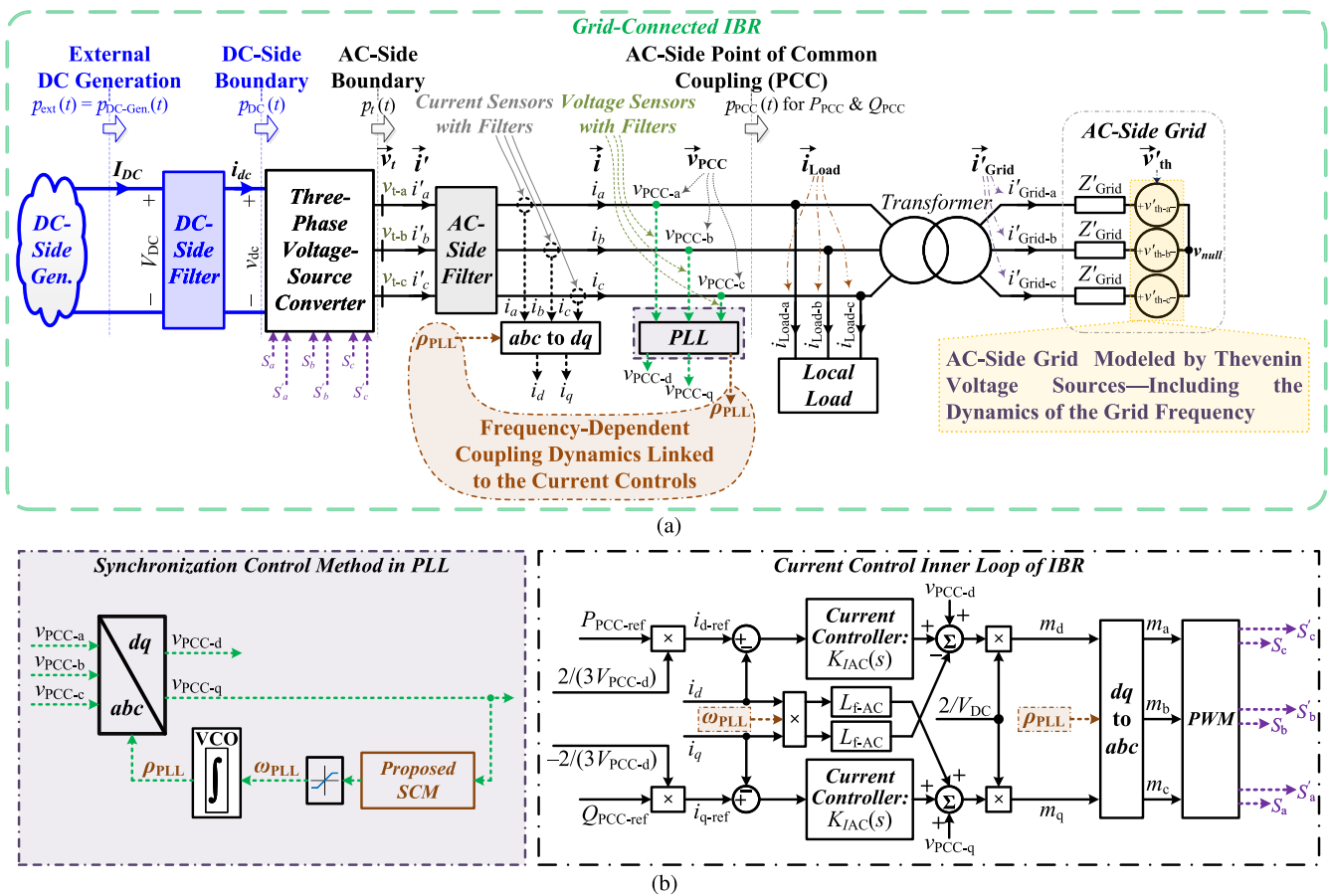


Fig. 1. (a) General structure of grid-connected IBRs and (b) current control and SCM showing how its dynamics impact the IBR's dynamics in modern grids with different grid impedance and inertia; L_{f-AC} represents the inductance of the IBR's ac-side filter.

and phase of \vec{i} , respectively; v_{t-dq} and $(\rho_{PLL} + \delta_2)$ represent the amplitude and phase of \vec{v}_t , respectively; $i_{Load-dq}$ and $(\rho_{PLL} + \delta_3)$ represent the amplitude and phase of \vec{i}_{Load} , respectively; and v_{th-dq} and $(\omega_{Grid}t + \theta_0)$ represent the amplitude and phase of \vec{v}_{th} , respectively. It is noteworthy that the subscript ‘PLL’ is employed to show that the phase generated is the outcome stabilized by an SCM in a commonly known PLL as the synchronization process. Afterward, using (3) and (4), one reaches (5) as follows.

$$\begin{aligned}
 & (1 + L_{GWQ})v_{PCC-dq}e^{j\rho_{PLL}} \\
 &= (R_{Grid} - R_{f-AC}L_{GWQ})i_{dq}e^{j(\rho_{PLL} + \delta_1)} \\
 &\quad - R_{Grid}i_{Load-dq}e^{j(\rho_{PLL} + \delta_3)} \\
 &\quad + L_{GWQ}v_{t-dq}e^{j(\rho_{PLL} + \delta_2)} \\
 &\quad - L_{Grid}\frac{d(i_{Load-dq}e^{j(\rho_{PLL} + \delta_3)})}{dt} \\
 &\quad + v_{th-dq}e^{j(\omega_{Grid}t + \theta_0)}. \tag{5}
 \end{aligned}$$

Before continuing the remaining mathematical manipulations, two angles should clearly be differentiated hereinafter. One is the angle generated by the synchronization process [which must follow the grid angle in transients (as much as possible) and steady state (for the final value in the time response)], and the other one is the grid angle. In this regard, ρ_{PLL} defines the former, and ρ_{Grid} expresses the latter to describe and encompass all of the required signals precisely.

In order to design a controller, a mathematical error signal is defined as follows, thereby helping synthesize SCM effectively.

$$\begin{aligned}
 e_\rho &\triangleq (\omega_{Grid}t + \theta_0) - \rho_{PLL} \\
 &= (\omega_{Grid}t + \theta_0 - \rho_{PLL}) \\
 &= (\rho_{Grid} - \rho_{PLL}) \\
 &= -(\rho_0 + \tilde{\rho}_{PLL} - \tilde{\rho}_{Grid}), \tag{6}
 \end{aligned}$$

where $\omega_{Grid}t + \theta_0$ is the grid angle which ρ_{Grid} expresses; ‘~’ shows the variation of a given signal around an operating point indicated by the subscript 0 hereinafter; ρ_0 is the angle generated by the synchronization process for one operating point; $\tilde{\rho}_{PLL}$ is the variation of the angle generated by the synchronization process around ρ_0 ; and $\tilde{\rho}_{Grid}$ is the variation of the grid angle caused by the limited value of the grid inertia—which gets impacted by low-inertia grids.

Then,

$$\begin{aligned}
 \frac{d\rho_{Grid}}{dt} - \frac{d\rho_{PLL}}{dt} &= \frac{d\tilde{\rho}_{Grid}}{dt} - \frac{d\tilde{\rho}_{PLL}}{dt} \\
 \Rightarrow \omega_{Grid} - \omega_{PLL} &= \tilde{\omega}_{Grid} - \tilde{\omega}_{PLL}. \tag{7}
 \end{aligned}$$

Now, if $\omega_{Grid} \triangleq \omega_0 + \tilde{\omega}_{Grid}$, which is considering the frequency fluctuations in low-inertia grids, one can conclude that

$$\omega_{PLL} = \omega_0 + \tilde{\omega}_{PLL} - \tilde{\omega}_{Grid}. \tag{8}$$

TABLE I
PARAMETERS OF FIGS. 1 AND 9

Parameter	Value	Parameter	Value
SCCR ^{see 1}	1.00	L_{f1}	1.1 mH
R_{f1}	0.01 Ω	L_{f2}	1.1 mH
R_{f2}	0.01 Ω	C_f	15.40 μ F
R_f	2.08 m Ω	f_s ^{see 5}	8.1 kHz
V_{DC} ^{see 2}	400 V	$V_{PCC\text{Line-to-Line rms}}$ ^{see 2}	208 V
H ^{see 3}	1.00 MJ/MVA	τ_g ^{see 6}	0.1 s
k_f ^{see 4}	$\frac{2S_n}{0.03f_{\text{Grid}}}$	k_p ^{see 7}	8×10^{-5}

¹ For calculating Z_{Grid} [16]. ⁵ Frequency Droop Coefficient [35]

² Nominal Value

⁶ Governor Time Constant [35]

³ Inertia Constant [35]

⁷ Damping Coefficient [35]

⁴ Switching Frequency

Considering that the variations of the variables with *Tilde* are not significant, the following trigonometric approximations are valid and are able to capture the linearized dynamics effectively.

$$\cos(\rho_0 + \tilde{\rho}_{\text{PLL}} - \tilde{\rho}_{\text{Grid}}) \approx \cos(\rho_0) - \sin(\rho_0)(\tilde{\rho}_{\text{PLL}} - \tilde{\rho}_{\text{Grid}}),$$

and

$$\sin(\rho_0 + \tilde{\rho}_{\text{PLL}} - \tilde{\rho}_{\text{Grid}}) \approx \sin(\rho_0) + \cos(\rho_0)(\tilde{\rho}_{\text{PLL}} - \tilde{\rho}_{\text{Grid}}). \quad (9)$$

After combining (5)–(9), (10)–(12) are obtained accordingly. They are able to describe the detailed PLL dynamics considering all variables or disturbance signals impacting the IBR's synchronization process—e.g., filter parameters, resistive and inductive parts of the grid impedance, grid frequency, and local load's and IBR's operating points—as detailed in (10) formatted in a single column.

$$\begin{aligned} \tilde{\rho}_{\text{PLL}}(s) &= \frac{1 + L_{\text{GWQ}}}{B(s)} \tilde{v}_{\text{PCC-q}}(s) - \frac{\sin(\delta_1)(R_{\text{Grid}} - R_{\text{f-AC}}L_{\text{GWQ}})}{B(s)} \tilde{i}_d(s) - \frac{\cos(\delta_1)(R_{\text{Grid}} - R_{\text{f-AC}}L_{\text{GWQ}})}{B(s)} \tilde{i}_q(s) \\ &+ \frac{(L_{\text{Grid}} \sin(\delta_3))s + (R_{\text{Grid}} \sin(\delta_3) + \omega_0 L_{\text{Grid}} \cos(\delta_3))}{B(s)} \tilde{i}_{\text{Load-d}}(s) \\ &+ \frac{(L_{\text{Grid}} \cos(\delta_3))s + (R_{\text{Grid}} \cos(\delta_3) - \omega_0 L_{\text{Grid}} \sin(\delta_3))}{B(s)} \tilde{i}_{\text{Load-q}}(s) \\ &- \frac{L_{\text{GWQ}} \sin(\delta_2)}{B(s)} \tilde{v}_{\text{t-d}}(s) - \frac{L_{\text{GWQ}} \cos(\delta_2)}{B(s)} \tilde{v}_{\text{t-q}}(s) + \tilde{\rho}_{\text{Grid}}(s), \\ &\triangleq \frac{N_1}{B(s)} \tilde{v}_{\text{PCC-q}}(s) + \frac{N_2}{B(s)} \tilde{i}_d(s) + \frac{N_3}{B(s)} \tilde{i}_q(s) + \frac{N_4 s + N_5}{B(s)} \tilde{i}_{\text{Load-d}}(s) + \frac{N_6 s + N_7}{B(s)} \tilde{i}_{\text{Load-q}}(s) \\ &+ \frac{N_8}{B(s)} \tilde{v}_{\text{t-d}}(s) + \frac{N_9}{B(s)} \tilde{v}_{\text{t-q}}(s) + \tilde{\rho}_{\text{Grid}}(s), \end{aligned} \quad (10)$$

where

$$B(s) = (L_{\text{Grid}} \sin(\delta_3) i_{\text{Load-q0}} - L_{\text{Grid}} \cos(\delta_3) i_{\text{Load-d0}})s - V_{\text{th}} \cos(\rho_0) \triangleq B_1 s - B_2, \quad (11)$$

in which

$$\begin{aligned} V_{\text{th}} \cos(\rho_0) &= (1 + L_{\text{GWQ}}) V_{\text{PCC-d0}} - (R_{\text{Grid}} - R_{\text{f-AC}}L_{\text{GWQ}})(\cos(\delta_1) i_{\text{d0}} - \sin(\delta_1) i_{\text{q0}}) \\ &+ R_{\text{Grid}}(\cos(\delta_3) i_{\text{Load-d0}} - \sin(\delta_3) i_{\text{Load-q0}}) \\ &- L_{\text{GWQ}}(\cos(\delta_2) V_{\text{t-d0}} - \sin(\delta_2) V_{\text{t-q0}}) - \omega_0 L_{\text{Grid}} \cos(\delta_3) i_{\text{Load-q0}} - \omega_0 L_{\text{Grid}} \sin(\delta_3) i_{\text{Load-d0}} \end{aligned} \quad (12)$$

B. Model Validation

Fig. 1 is simulated (with the parameters reported in Table I) for model validation in this subsection. To this end, the commonly known active/reactive power control [based on the current-controlled methodology using the pulse width modulation switching scheme] is used so that P_{PCC} tracks $P_{\text{PCC-ref}}$ and Q_{PCC} tracks $Q_{\text{PCC-ref}}$ with a reasonable bandwidth; in this regard, i_d reaches $i_{d\text{-ref}}$ and i_q reaches $i_{q\text{-ref}}$. Based on the operation of a grid-connected IBR using the method mentioned above (which benefits from a decoupled active/reactive power control through the synchronization process), the reference signals of $i_{d\text{-ref}}$ and $i_{q\text{-ref}}$ are described as $\frac{2P_{\text{PCC-ref}}}{3v_{\text{PCCd}}}$ and $\frac{-2Q_{\text{PCC-ref}}}{3v_{\text{PCCd}}}$, respectively. Equations (10)–(12), as shown at the bottom of the page, (written in the one-column format) describe the dynamics derived in this research. In order to validate them, two model validation test cases have been examined as follows.

1) *Model Validation Test Case I*: First, the grid-connected IBR's active/reactive power is set to 10 kW/5 kvar, the active power is increased by 10% at $t = 2.0$ s (while the reactive power is set to the last value), and the active power is increased by 5% at $t = 2.5$ s (while the active power is set to the last value). Fig. 2(a) shows the nonlinear and linear models' results of the model validation Test Case I and reveals good agreement between the simulations, thereby validating the derived dynamic model.

2) *Model Validation Test Case II*: Second, the reverse process is carried out for the active power, so it is decreased by 10% at $t = 3.0$ s (while the reactive power is set to the last value). Fig. 2(b) shows the nonlinear and linear models' results of the model validation Test Case II and displays good agreement between the simulations, thereby validating the derived dynamic model.

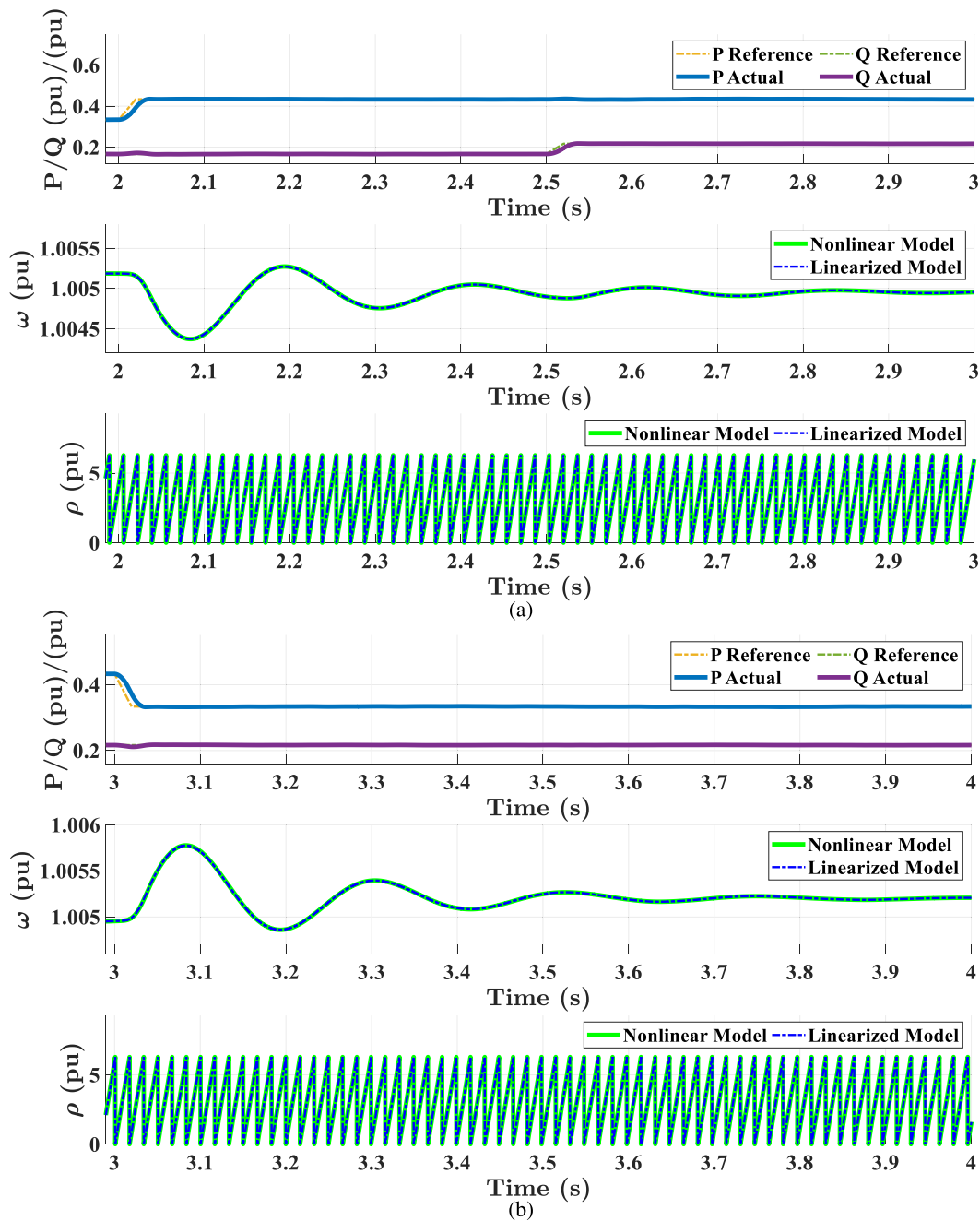


Fig. 2. Model validation results of (10): (a) Model Validation Test Case I and (b) Model Validation Test Case II.

III. PROPOSED CONTROL DESIGN

This section develops an adaptive optimal control algorithm based on the ADP and the internal model principle for SCM. In this regard, a remarkable advantage is that the system dynamics are not required to be known accurately for optimal controller design. It is noteworthy that knowing how to design a model-based optimal controller is first needed, as detailed in this section. To this end, first, the synchronization process's dynamic model is described in the state-space representation. Then, a model-based optimal controller is designed. Finally, a model-free adaptive optimal control is synthesized and provided as a solution to SCM.

A. State-Space Model of the PLL Dynamics

Taking the Laplace inverse transform of (10), the following is obtained.

$$\begin{aligned}
 & B_1(\dot{\tilde{\rho}}_{PLL}(t) - \dot{\tilde{\rho}}_{Grid}(t)) + B_2(\tilde{\rho}_{PLL}(t) - \tilde{\rho}_{Grid}(t)) \\
 &= N_1 \tilde{v}_{PCC-q}(t) + N_2 \tilde{i}_d + N_3 \tilde{i}_q + N_4 \tilde{i}_{Load-d}(t) + N_5 \tilde{i}_{Load-d}(t) \\
 & \quad + N_6 \tilde{i}_{Load-q}(t) + N_7 \tilde{i}_{Load-q}(t) + N_8 \tilde{v}_{t-d} + N_9 \tilde{v}_{t-q}. \quad (13)
 \end{aligned}$$

Let the state be $x(t) = \tilde{\rho}_{PLL}(t) - \tilde{\rho}_{Grid}(t)$ and the input be $u(t) = \tilde{v}_{PCC-q}(t)$ to follow the standard SCM. Therefore, a continuous-time state-space model describes the differential

equation, as expressed in (14).

$$\dot{x}(t) = A_c x(t) + B_c u(t) + d_1 + d_2(t) + d_3(t), \quad (14)$$

where $A_c \triangleq -\frac{B_2}{B_1}$, $B_c \triangleq \frac{N_1}{B_1}$, $d_1 \triangleq \frac{1}{B_1}(N_2\tilde{i}_d + N_3\tilde{i}_q + N_8\tilde{v}_{t-d} + N_9\tilde{v}_{t-q})$, and $d_2(t) \triangleq \frac{1}{B_1}(N_4\dot{\tilde{i}}_{\text{Load-d}}(t) + N_5\dot{\tilde{i}}_{\text{Load-d}}(t) + N_6\dot{\tilde{i}}_{\text{Load-q}}(t) + N_7\dot{\tilde{i}}_{\text{Load-q}}(t))$.

In case there are any unbalanced conditions in PCC voltages, the load current's dq -components of $\tilde{i}_{\text{Load-d}}(t)$ and $\tilde{i}_{\text{Load-q}}(t)$ will include sinusoidal signals in the angular frequency of $2\omega_0$. Since there is a chance that it happens (when the PCC voltage gets unbalanced), it is obvious that $d_2(t)$ is also a sinusoidal signal in that frequency (i.e., $2f_0$) or equivalently in the angular frequency of $2\omega_0$. One can define it as $d_2(t) = d_{21} \sin(2\omega_0 t) + d_{22} \cos(2\omega_0 t)$.

The disturbance of $d_3(t)$ is included in order to consider a ramp function or sawtooth wave. The internal model principle requires the controller to include $d_3(t)$ for either ramp function or sawtooth wave. They are required because of the nature of the reference signal induced by the integral of the angular frequency (for ramp function) or the voltage-controlled oscillator (commonly known as VCO) included after the integrator component (for the sawtooth wave) to get the synchronization angle from the block diagram of the synchronization process. In this regard, suppose that the period of the sawtooth wave is T_3 (i.e., $\frac{1}{60}$ s in power systems) and its slope is d_{31} (i.e., $\frac{2\pi}{60} = 120\pi$ rad/s in power systems). Therefore, for any $n = 0, 1, 2, \dots$, the time derivative of $d_3(t)$, i.e., $\dot{d}_3(t)$, is described as

$$\dot{d}_3(t) = \begin{cases} d_{31}, & t \in [2nT_3, (2n+1)T_3) \\ -d_{31}, & t \in [(2n+1)T_3, (2n+2)T_3) \end{cases} \quad (15)$$

Since the sawtooth wave can be considered as a piecewise ramp signal—without loss of generality—the state-space model is found for any t in the first half period, i.e., $\forall t \in [0, T_3)$. The state-space model for any $t \geq T_3$ can be obtained by slight modification. Moreover, by the fact that d_1 is a constant, the disturbances $d(t) \triangleq d_1 + d_2(t) + d_3(t)$ can be generated by the following autonomous system

$$\begin{aligned} \dot{w}(t) &= A_{1c} w(t), \\ d(t) &= E_c w(t), \end{aligned} \quad (16)$$

where the initial value is $w(0) = [0, 1, 0, 1]^T$, and

$$A_{1c} = \begin{bmatrix} 0 & d_{31} & 0 & 0 \\ 0 & 0 & 0 & 0 \\ 0 & 0 & 0 & 2\omega_0 \\ 0 & 0 & -2\omega_0 & 0 \end{bmatrix}, \quad E_c = [1 \ d_1 \ d_{21} \ d_{22}]. \quad (17)$$

Remark 1: Note that the autonomous system (16), also called exosystem in the ADP-based control theories, can also be employed to generate harmonics. As a result, it is able to consider the PCC voltages with harmonics for any sequence of interest. For instance, consider the fifth-order harmonic in the abc sequence (equivalent to $6\omega_0$ in the dq -frame) and the eleventh-order harmonic in the abc sequence (identical to $12\omega_0$ in the dq -frame) as the disturbance signals. Then, one

can revise the exosystem state matrix by A'_{1c} , which is a block diagonal matrix of A_{1c} and A_{2c} , where

$$A_{2c} = \begin{bmatrix} 0 & 6\omega_0 & 0 & 0 \\ -6\omega_0 & 0 & 0 & 0 \\ 0 & 0 & 0 & 12\omega_0 \\ 0 & 0 & -12\omega_0 & 0 \end{bmatrix}. \quad (18)$$

By combining (14) and (16), a complete continuous-time synchronization process's system model is obtained as follows.

$$\begin{aligned} \dot{w}(t) &= A_{1c} w(t), \quad \text{and} \\ \dot{x}(t) &= A_c x(t) + B_c u(t) + E_c w(t). \end{aligned} \quad (19)$$

Choosing a non-pathological sampling period T_s [36], the continuous-time system (19) can be discretized as follows

$$w_{k+1} = A_1 w_k, \quad \text{and} \quad (20)$$

$$x_{k+1} = A x_k + B u_k + E w_k, \quad (21)$$

where system matrices are

$$A = e^{A_c T_s},$$

$$B = \left(\int_0^{T_s} e^{A_c \tau} d\tau \right) B_c,$$

$$E = \left(\int_0^{T_s} e^{A_c \tau} d\tau \right) E_c.$$

B. Model-Based Optimal Controller Design

In this paper, the SCM objective is to design an optimal controller such that the closed-loop system is asymptotically stable while rejecting the external disturbance $E w_k$. Moreover, the controller should be designed without the knowledge of system dynamics, i.e., A , B , and E . Before achieving this goal, it is necessary to know how to design a model-based optimal controller for the synchronization process.

Note that since there are sinusoidal signals in the disturbance, a simple application of proportional-integral controller design cannot reject the disturbance. As a result, the notion of the internal model is introduced. To be more specific, $G = [1 \ 1 \ 1 \ 1]^T$ is defined. It is easy to double-check that the pair (A_1, G) is controllable for any frequency $2\omega_0 > 0$. By the internal model principle [37], the pair (A_1, G) is an internal model of the exosystem (20).

The following Lemma shows that the disturbance in the synchronization process defined in (21) can be rejected by developing a state-feedback controller.

Lemma 1: The system (21) is asymptotically stable if one develops a dynamic state-feedback controller in the form of

$$\begin{aligned} u_k &= -K_x x_k - K_z z_k \\ z_{k+1} &= A_1 z_k + G x_k, \end{aligned} \quad (22)$$

ensuring that $\begin{bmatrix} A - B K_x & -B K_z \\ G & A_1 \end{bmatrix}$ is a Schur matrix.

Proof: By the synchronization process, it is known that $B \neq 0$. This matter shows that for any eigenvalue λ of the matrix A_1 , the following matrix always has full rank, i.e.,

$$\text{rank} \begin{bmatrix} A - \lambda B & B \\ 1 & 0 \end{bmatrix} = 2,$$

thus immediately implying that the zero-transmissions condition holds.

Based on the output regulation theory, there always exists a unique vector $X \in \mathbb{R}^{1 \times 5}$ and a constant $U \in \mathbb{R}^{1 \times 5}$ solving the following matrix equations

$$XA_1 = AX + BU + E, \text{ and} \quad (23)$$

$$X = 0. \quad (24)$$

Moreover, from [38, Lemma 1.38], there always exist a unique solution (\hat{X}, Z) solving (24) and

$$\begin{aligned} \hat{X}A_1 &= (A - BK_x)\hat{X} - BK_zZ + E, \text{ and} \\ ZA_1 &= A_1Z + G\hat{X}. \end{aligned} \quad (25)$$

Therefore, $X = \hat{X} = 0$ and $U = -K_zZ$ are concluded. Provided that

$$\begin{aligned} \bar{z}_k &= z_k - Zw_k, \text{ and} \\ \bar{u}_k &= u_k - Uw_k \triangleq -K_x x_k - K_z \bar{z}_k, \end{aligned} \quad (26)$$

the system (21)–(22) can be transformed by

$$\begin{bmatrix} \bar{x}_{k+1} \\ \bar{z}_{k+1} \end{bmatrix} = \begin{bmatrix} A - BK_x & -BK_z \\ G & A_1 \end{bmatrix} \begin{bmatrix} \bar{x}_k \\ \bar{z}_k \end{bmatrix}. \quad (27)$$

It is evident that the system (27) is asymptotically stable at the origin, thus indicating that $\lim_{k \rightarrow \infty} x_k = 0$. The proof is thus completed. ■

The controller is further synthesized in order to minimize the following quadratic cost by considering optimal design.

$$\min_{\bar{u}_k} \sum_{k=0}^{\infty} \left(\begin{bmatrix} x_k \\ \bar{z}_k \end{bmatrix}^T Q \begin{bmatrix} x_k \\ \bar{z}_k \end{bmatrix} + R\bar{u}_k^2 \right) \quad (28)$$

$$\text{subject to } \begin{bmatrix} x_{k+1} \\ \bar{z}_{k+1} \end{bmatrix} = \bar{A} \begin{bmatrix} x_k \\ \bar{z}_k \end{bmatrix} + \bar{B}\bar{u}_k, \quad (29)$$

where $Q \in \mathbb{R}^{5 \times 5}$ and $R \in \mathbb{R}$ are symmetric and positive definite, and

$$\bar{A} = \begin{bmatrix} A & 0 \\ G & A_1 \end{bmatrix}, \quad \bar{B} = \begin{bmatrix} B \\ 0 \end{bmatrix}.$$

By linear optimal control theory, the optimal controller that minimizes (28) is

$$\bar{u}_k = -K_x^* \bar{x}_k - K_z^* \bar{z}_k. \quad (30)$$

The optimal feedback control gain $K^* = [K_x^* \ K_z^*]$ is

$$K^* = (R + \bar{B}^T P^* \bar{B})^{-1} \bar{B}^T P^* \bar{A},$$

where the matrix $P^* = (P^*)^T > 0$ uniquely solves the following Riccati equation.

$$\bar{A}^T P^* \bar{A} - P^* + \bar{Q} - \bar{A}^T P^* \bar{B} (R + \bar{B}^T P^* \bar{B})^{-1} \bar{B}^T P^* \bar{A} = 0. \quad (31)$$

C. Model-Free Optimal Controller Design

This section proposes and synthesizes a model-free optimal control approach to the synchronization process with unknown system dynamics A , B , and E . In order to begin with, $\xi_k = [x_k^T, z_k^T]^T$ is defined. The original discrete-time system (20) with the internal model (22) can be rewritten by

$$\xi_{k+1} = \bar{A}\xi_k + \bar{B}u_k + \bar{E}w_k, \quad (32)$$

where $\bar{E} = [E \ 0]^T$.

The proposed approach is based on Q -learning [39]. A quadratic, state-input dependent function $\mathcal{Q}_j(\xi_k, u_k, w_k)$ is defined and named Q -function as follows.

$$\begin{aligned} \mathcal{Q}_j(\xi_k, u_k, w_k) &= \begin{bmatrix} \xi_k \\ u_k \\ w_k \end{bmatrix}^T \begin{bmatrix} \bar{A}^T P_j \bar{A} & \bar{A}^T P_j \bar{B} & \bar{A}^T P_j \bar{E} \\ \bar{B}^T P_j \bar{A} & \bar{B}^T P_j \bar{B} & \bar{B}^T P_j \bar{E} \\ \bar{E}^T P_j \bar{A} & \bar{E}^T P_j \bar{B} & \bar{E}^T P_j \bar{E} \end{bmatrix} \begin{bmatrix} \xi_k \\ u_k \\ w_k \end{bmatrix}. \end{aligned} \quad (33)$$

Also, the following symmetric matrix is defined.

$$\begin{aligned} \mathcal{P}_j &= \begin{bmatrix} \mathcal{P}_j[1, 1] & \mathcal{P}_j[1, 2] & \mathcal{P}_j[1, 3] \\ (\mathcal{P}_j[1, 2])^T & \mathcal{P}_j[2, 2] & \mathcal{P}_j[2, 3] \\ (\mathcal{P}_j[1, 3])^T & (\mathcal{P}_j[2, 3])^T & \mathcal{P}_j[3, 3] \end{bmatrix} \\ &\triangleq \begin{bmatrix} \bar{A}^T P_j \bar{A} & \bar{A}^T P_j \bar{B} & \bar{A}^T P_j \bar{E} \\ \bar{B}^T P_j \bar{A} & \bar{B}^T P_j \bar{B} & \bar{B}^T P_j \bar{E} \\ \bar{E}^T P_j \bar{A} & \bar{E}^T P_j \bar{B} & \bar{E}^T P_j \bar{E} \end{bmatrix}, \end{aligned} \quad (34)$$

where j stands for the learning iteration discussed in learning Algorithm 1. Next, the value-iteration-based ADP algorithm is proposed in Algorithm 1, which does not rely on an initial stabilizing control gain.

Algorithm 1 Model-Free Optimal Control Algorithm

- 1: $j \leftarrow 0$, $\mathcal{P}_j \leftarrow 0$, $K_j \leftarrow 0$. Pick a $\epsilon > 0$.
 - 2: Apply an arbitrary control policy u_k for $k \in [0, T]$ such that the signal (ξ_k, u_k, w_k) is persistently excited.
 - 3: **repeat**
 - 4: Solve \mathcal{P}_{j+1} via least squares from

$$\mathcal{Q}_{j+1}(\xi_k, u_k, w_k) = \mathcal{Q}_j(\xi_{k+1}, -K_j \xi_{k+1}, 0) + \xi_k^T (Q + K_j^T R K_j) \xi_k \quad (35)$$
 - 5: Solve K_{j+1} by

$$K_{j+1} \leftarrow (\mathcal{P}_{j+1}[2, 1]) / (R + \mathcal{P}_{j+1}[2, 2]) \quad (36)$$
 - 6: $j \leftarrow j + 1$
 - 7: **until** $|\mathcal{P}_j - \mathcal{P}_{j-1}| < \epsilon$
 - 8: $j^* \leftarrow j$.
-

Remark 2: Similar to the existing work in reinforcement learning and adaptive control, the learning Algorithm 1 needs the online collected data to be persistently excited. In this paper, the signals $\{\xi_k, u_k, w_k\}_{k=0}^T$ are persistently excited if the following rank condition holds

$$\text{rank} \begin{bmatrix} [\xi_0^T, u_0^T, w_0^T] \otimes [\xi_0^T, u_0^T, w_0^T] \\ [\xi_1^T, u_1^T, w_1^T] \otimes [\xi_1^T, u_1^T, w_1^T] \\ \vdots \\ [\xi_{T-1}^T, u_{T-1}^T, w_{T-1}^T] \otimes [\xi_{T-1}^T, u_{T-1}^T, w_{T-1}^T] \end{bmatrix}$$

$$= \frac{10(10+1)}{2}, \quad (37)$$

where \otimes is the Kronecker product operator.

Remark 3: Different from existing ADP methods [40], [41], [42] for stabilization problems, Algorithm 1 can be employed to explore the optimal control policy of systems with the presence of external signals. Algorithm 1 effectively combines the internal model principle, output regulation theory, and ADP techniques.

D. Convergence and Stability Analysis

The convergence of the proposed Algorithm 1 is analyzed in the following theorem.

Theorem 1: Sequences $\{\mathcal{P}_j\}_{j=0}^{\infty}$ and $\{K_j\}_{j=0}^{\infty}$ obtained from solving Algorithm 1 converge to \mathcal{P}^* and K^* , where

$$\mathcal{P}^* = \begin{bmatrix} \bar{A}^T P^* \bar{A} & \bar{A}^T P^* \bar{B} & \bar{A}^T P^* \bar{E} \\ \bar{B}^T P^* \bar{A} & \bar{B}^T P^* \bar{B} & \bar{B}^T P^* \bar{E} \\ \bar{E}^T P^* \bar{A} & \bar{E}^T P^* \bar{B} & \bar{E}^T P^* \bar{E} \end{bmatrix}.$$

Proof: Mathematical induction is considered in order to prove this fact.

- 1) Let $j = 0$. Since the signal (ξ_k, u_k, w_k) is persistently excited, one can uniquely solve a symmetric matrix \mathcal{P}_1 from (35) given $\mathcal{P}_0 = 0$. Based on the definition of Q -function in (33), (35) is equivalent to

$$\xi_{k+1}^T P_1 \xi_{k+1} = \xi_{k+1}^T [(A - BK_0)^T P_0 (A - BK_0) + Q + K_0^T R K_0] \xi_{k+1}. \quad (38)$$

One can immediately obtain that any matrix $\hat{\mathcal{P}}_1$ satisfying the following equations is a solution to (35).

$$\hat{\mathcal{P}}_1 = \begin{bmatrix} \bar{A}^T \hat{P}_1 \bar{A} & \bar{A}^T \hat{P}_1 \bar{B} & \bar{A}^T \hat{P}_1 \bar{E} \\ \bar{B}^T \hat{P}_1 \bar{A} & \bar{B}^T \hat{P}_1 \bar{B} & \bar{B}^T \hat{P}_1 \bar{E} \\ \bar{E}^T \hat{P}_1 \bar{A} & \bar{E}^T \hat{P}_1 \bar{B} & \bar{E}^T \hat{P}_1 \bar{E} \end{bmatrix}, \text{ and}$$

$$\hat{P}_1 = (A - BK_0)^T P_0 (A - BK_0) + Q + K_0^T R K_0.$$

Due to the uniqueness of the solution to (35), $\mathcal{P}_1 = \hat{\mathcal{P}}_1$ and $P_1 = \hat{P}_1$ are inferred. Then, K_1 is further solved by (36), which is equivalent to

$$\hat{K}_1 = (R + \bar{B}^T P_1 \bar{B})^{-1} \bar{B}^T P_1 \bar{A}.$$

- 2) Let $j = i$. Suppose the triple $(P_i, \mathcal{P}_i, K_i)$; solving from Algorithm 1 satisfies $P_i = \hat{P}_i$, $\mathcal{P}_i = \hat{\mathcal{P}}_i$, and $K_i = \hat{K}_i$. As a result, the triple $(\hat{P}_i, \hat{\mathcal{P}}_i, \hat{K}_i)$ satisfies the following equations.

$$\begin{aligned} \hat{\mathcal{P}}_i &= \begin{bmatrix} \bar{A}^T \hat{P}_i \bar{A} & \bar{A}^T \hat{P}_i \bar{B} & \bar{A}^T \hat{P}_i \bar{E} \\ \bar{B}^T \hat{P}_i \bar{A} & \bar{B}^T \hat{P}_i \bar{B} & \bar{B}^T \hat{P}_i \bar{E} \\ \bar{E}^T \hat{P}_i \bar{A} & \bar{E}^T \hat{P}_i \bar{B} & \bar{E}^T \hat{P}_i \bar{E} \end{bmatrix}, \\ \hat{P}_i &= (A - BK_{i-1})^T P_{i-1} (A - BK_{i-1}) \\ &\quad + Q + K_{i-1}^T R K_{i-1}, \text{ and} \\ \hat{K}_i &= (R + \bar{B}^T P_i \bar{B})^{-1} \bar{B}^T P_i \bar{A}. \end{aligned} \quad (39)$$

Since the signal (ξ_k, u_k, w_k) is persistently excited, one can uniquely solve a symmetric matrix \mathcal{P}_{i+1} from (35) given \mathcal{P}_i . Similar to $j = 0$, one can immediately

obtain that any matrix $\hat{\mathcal{P}}_{i+1}$ is satisfying the following equations.

$$\hat{\mathcal{P}}_{i+1} = \begin{bmatrix} \bar{A}^T \hat{P}_i \bar{A} & \bar{A}^T \hat{P}_i \bar{B} & \bar{A}^T \hat{P}_i \bar{E} \\ \bar{B}^T \hat{P}_i \bar{A} & \bar{B}^T \hat{P}_i \bar{B} & \bar{B}^T \hat{P}_i \bar{E} \\ \bar{E}^T \hat{P}_i \bar{A} & \bar{E}^T \hat{P}_i \bar{B} & \bar{E}^T \hat{P}_i \bar{E} \end{bmatrix}, \text{ and}$$

$$\hat{P}_{i+1} = (A - BK_i)^T P_i (A - BK_i) + Q + K_i^T R K_i,$$

which is a solution to (35). Due to the uniqueness of the solution to (35), $\mathcal{P}_{i+1} = \hat{\mathcal{P}}_{i+1}$ and $P_{i+1} = \hat{P}_{i+1}$ are found. Then, $K_{i+1} = \hat{K}_{i+1}$ is obtained, where \hat{K}_{i+1} is

$$\hat{K}_{i+1} = (R + \bar{B}^T P_i \bar{B})^{-1} \bar{B}^T P_i \bar{A}.$$

- 3) The authors of [43] have shown that the sequences $\{\hat{P}_j\}_{j=0}^{\infty}$ and $\{\hat{K}_j\}_{j=0}^{\infty}$ converge to the optimal values P^* and K^* . Finally, one can conclude that $\lim_{j \rightarrow \infty} \mathcal{P}_j = \mathcal{P}^*$, $\lim_{j \rightarrow \infty} K_j = K^*$.

The proof is thus completed. \blacksquare

The closed-loop system stability is next shown and proved in the following theorem.

Theorem 2: Given a control gain K_j^* learned from Algorithm 1, the control policy

$$\bar{u}_k = -K_j^* w_k \quad (40)$$

asymptotically stabilizes the system (21).

Proof: The system (21) in closed-loop with the approximated controller (40) satisfies

$$\begin{bmatrix} x_{k+1} \\ \bar{z}_{k+1} \end{bmatrix} = (\bar{A} - \bar{B} K_j^*) \begin{bmatrix} x_k \\ \bar{z}_k \end{bmatrix}.$$

Due to the fact that $\bar{A} - \bar{B} K^*$ is a Schur matrix and that the convergence of the sequence $\{K_j\}_{j=0}^{\infty}$, there always exists a small enough threshold $\epsilon > 0$ in Algorithm 1 such that $\bar{A} - \bar{B} K_j^*$ is Schur, which implies that $\lim_{k \rightarrow \infty} \bar{x}_k = 0$ and $\lim_{k \rightarrow \infty} \bar{z}_k = 0$. The proof is thus completed. \blacksquare

Remark 4: It is worth mentioning that only the frequency content of disturbance must be known when applying the proposed controller to the synchronization process dynamics described in (10). As the proposed method is a data-driven approach that does not rely on the model knowledge, any further information on the synchronization process system dynamics may not improve the performance of controller synthesis.

IV. SIMULATIONS AND EXPERIMENTS

This section provides the results of both simulations and experiments. In this regard, the proposed methodology for different grid conditions is simulated as follows. Fig. 1, whose parameters are reported in Table I, has been tested in MATLAB Simulink. Thevenin's equivalent circuit is deployed to model the grid, as depicted in Fig. 1. It is worthy of mention that the voltage source amplitude equals the grid nominal voltage. The short circuit capacity (SCC) at PCC is defined as $\text{SCC}_{\text{PCC}} = \text{SCCR} \times S_{\text{VSC}}$, where S_{VSC} is the nominal power of the inverter connected to the grid. SCC_{PCC} is employed to determine the values of the passive components

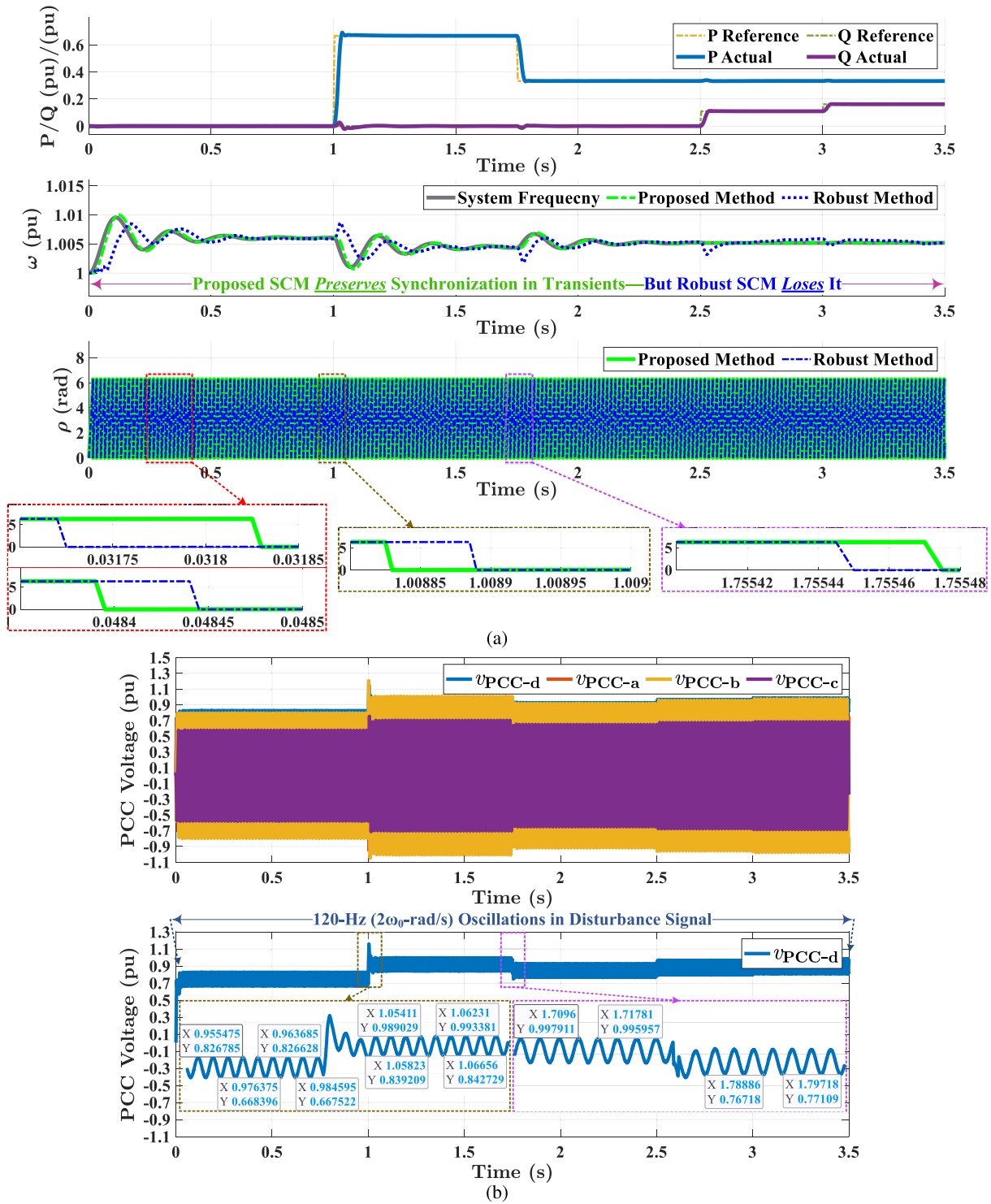


Fig. 3. Simulation results of Test Case I: (a) Control response to changes in the grid-connected IBR's operating point power and (b) the disturbance signal without distortion.

associated with Z_{Grid} . In order to consider L_{Grid} and R_{Grid} components in Z_{Grid} , this article has simulated the case resulting in one of the worst-case scenarios for the power transfer from/to a grid-connected IBR to/from an ac grid, as detailed in [16], [44].

In addition to the grid impedance, the equivalent moment of inertia J (or equivalently inertia constant H) is another factor for getting weak grids. This study uses one of the

practically lowest possible values of the inertia constant H (causing the lowest possible J). The control gains pertaining to the applied governors have been used. Using them and the highest possible grid impedance amplitude (and hence the lowest possible SCCR), the most fluctuating and yet practical frequency dynamics are made here. To this end, $H = 1$ (i.e., the low-inertia grid condition) is employed to make the grid low-inertia, and $SCCR = 1$ (i.e., the very weak grid condition)

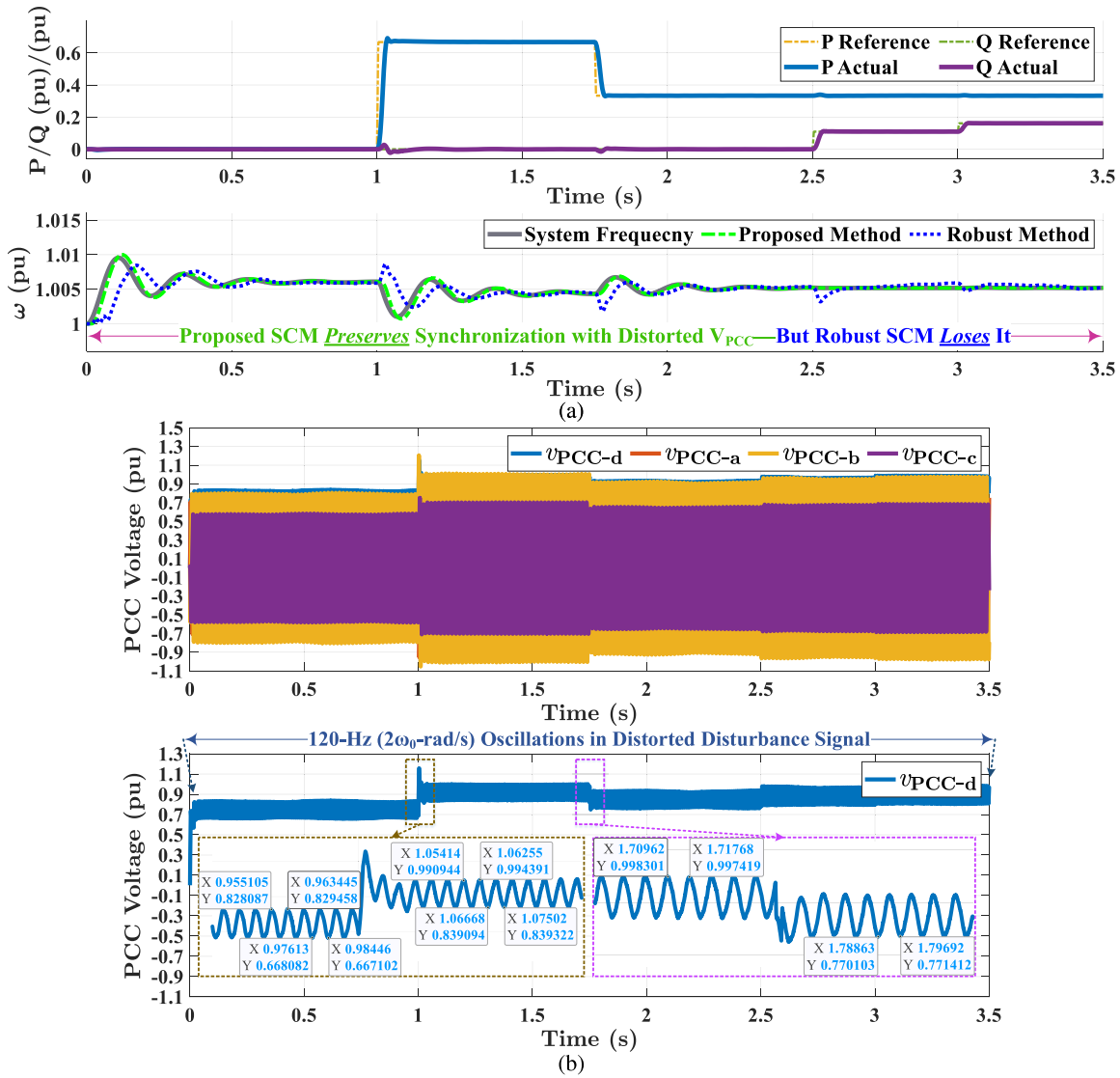


Fig. 4. Simulation results of Test Case II: (a) Control response to changes in the grid-connected IBR's operating point power and (b) the disturbance signal with distortions.

is considered in order to have the highest amount of grid impedance. Both practically make the grid as weak as possible in real-world cases. For the controller, the proposed controller detailed in Section III is initially designed and learned for $SCCR = 1$ and nominal power and tested as explained next. All other required parameters have been outlined in Table I.

A. Proposed Controller Simulated in Different Test Cases

1) *Test Case I:* As detailed here, a general test case has been considered (without loss of generality) for simulations. 15% decrease in Phase A and 30% decrease in Phase C have been taken into account for the PCC voltage amplitude. For this test case, the converter is connected and synchronized to the grid with active/reactive power of 0 kW/0 kvar. Then, at $t = 1$ s, the active power set-point is changed from 0 kW to 20 kW [i.e., 0.6667 per unit (pu)] while the reactive power is still 0 kvar [i.e., unity power factor (PF)]. Next, at $t = 1.75$ s, the active power is reduced from 20 kW to 10 kW (i.e., 0.3333 pu) (with $PF = 1$). Afterward, at $t = 2.50$ s, the reactive power set-point is increased from 0 kvar to 3.288 kvar (i.e., 0.1096 pu)

to make the $PF = 0.95$ while the active power is still 10 kW (i.e., 0.3333 pu). Finally, at $t = 3.00$ s, PF is decreased from 0.95 to 0.90 by altering the reactive power set-point from 3.288 kvar (i.e., 0.1096 pu) to 4.842 kvar (i.e., 0.1614 pu). Fig. 3 depicts the proposed method's results of Test Case I, including the disturbance signals.

Fig. 3 shows that the proposed method is able to track the reference of the frequency signal satisfactorily. During transients, the proposed controller is able to track the frequency of the grid effectively, meaning that the synchronization during transients is still preserved. This matter enables the converter to supply the demand with more improved transient responses—even for unbalanced, low-inertia, and very weak grids—thereby strengthening the synchronization process.

2) *Test Case II:* This test case repeats the events detailed in Test Case I but with distorted voltage to test the performance of the proposed controller while a filter gets cascaded with SCM in the PLL structure (e.g., the loop filter in [45]) to eliminate odd harmonics tuned at the 5th and 7th harmonics; it is noteworthy that the zero-sequence harmonics and the 11th,

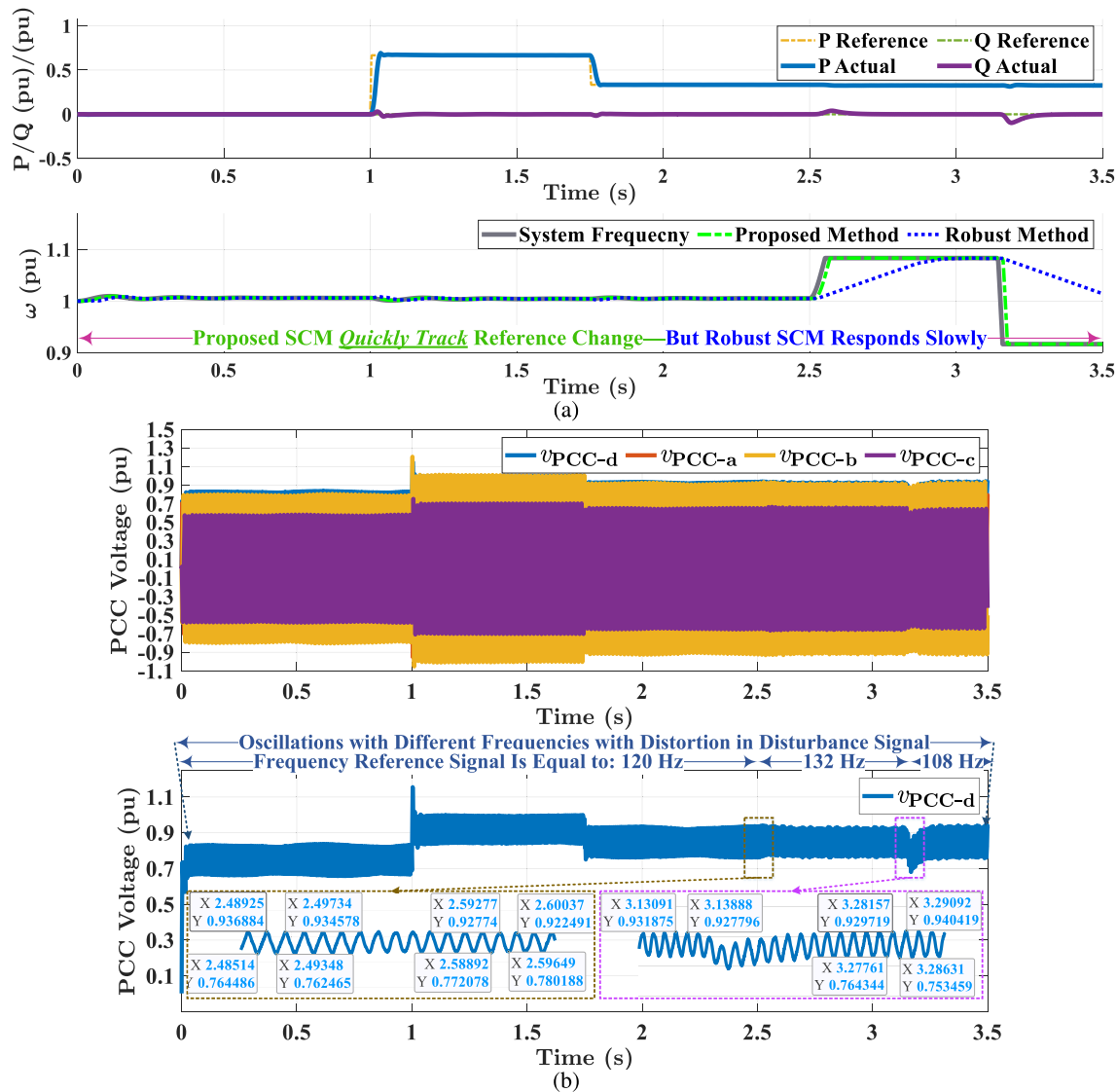


Fig. 5. Simulation results of Test Case III: (a) Control response to the system frequency change and (b) the disturbance signal with distortions.

$13^{\text{th}}, \dots, (2k+1)^{\text{th}}$ ($k \in \mathbb{N}$ and $k \neq 3m+1$ with $m \in \mathbb{N}$) ones are negligible per current grid designs without loss of generality. Fig. 4 displays the proposed method's results of Test Case II, including the disturbance signals. The results reveal that the proposed controller is capably able to perform as detailed in Test Case I—even when the PCC voltage is somewhat distorted—for which SCM in the PLL structure utilizes a commonly used filter.

3) *Test Case III*: This test case examines the response of the proposed controller to the frequency reference change with distorted PCC voltages, while the loop filter in Test Case II takes it into account. To this end, this test case includes the relevant loop filter in [45] and replicates Test Case II's events—i.e., those in Test Case I—except for two moments; at $t = 2.50$ s and $t = 3.15$ s, the frequency reference signal is changed to 1.1 pu and 0.9 pu, respectively, while the PF value remains 1. Fig. 5 presents the proposed method's results of Test Case III, including the disturbance signals. The results indicate that the controller proposed in this study effectively

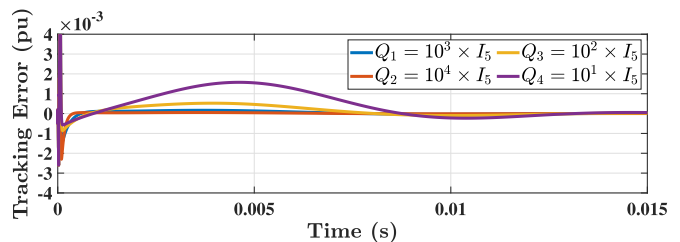


Fig. 6. Simulation results of the performance evaluation of the proposed controller, where I_5 is a 5×5 unity matrix.

tracks the reference signal. This matter is achieved despite the presence of reasonably distorted PCC voltage and the use of a filter commonly employed in SCM in the PLL structure.

B. Performance of the Proposed Controller

This section discusses and examines the performance of the proposed controller. As the ADP method is a data-driven version of the LQR design for linear systems, any guidelines

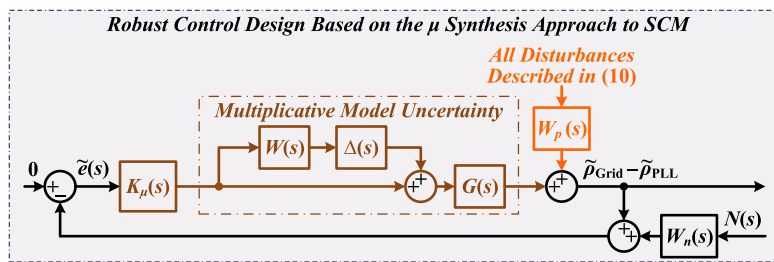


Fig. 7. Robust control design structure of the PLL SCM based on the μ synthesis approach.

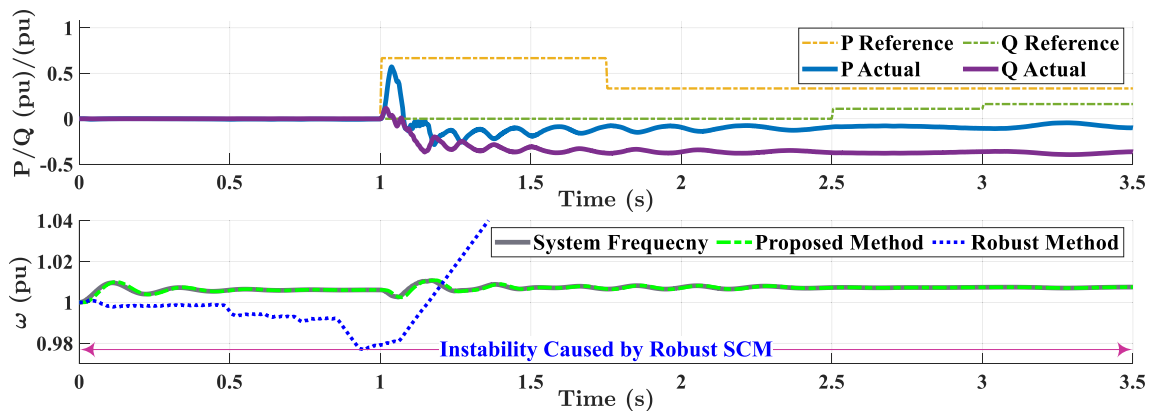


Fig. 8. Simulation results of the robust SCM's response to Test Case I.



Fig. 9. Test rig deployed in experiments.

on tuning the weight matrices Q and R in the LQR design apply to the ADP implementations. As depicted in Fig. 6, the matrix Q impacts the SCM performance. It reveals that a higher value for the Q coefficient results in quicker convergence of the tracking error—which aligns with the principles of linear optimal control theory.

C. Comparative Results Generated by Robust Control

For comparison purposes, Test Cases I–III are repeated for the controller synthesized in this subsection; its results

are depicted in Fig. 3–5 showing the results of the proposed controller and those of the controller for comparison. In this regard and in order to make a valid comparison, a robust controller has been designed according to the μ synthesis approach because a proportional-integral-derivative controller is unable to induce optimal performance necessarily (at least for the nominal conditions); it is too simple to do so. The methodological procedure of the μ -synthesis-based technique is employed to design a robust control. It deploys the so-called D - K iteration process, an iterative solution

to estimate and optimize the dynamic plant's robust H_∞ performance.

The MATLAB software is deployed to perform the D - K iteration process in this subsection. Other publications provide detailed information on how to apply that method in voltage-source/sourced converters (e.g., see [11], [12], [14], [46], [47], [48]). Besides, its theoretical background is provided in different kinds of literature on control theories [49], [50]. Following the procedure detailed by the authors in [11], [14], [46], [47], [48] while considering the required problem formulation for the robust control design (demonstrated in Fig. 7), a robust SCM based on the μ synthesis technique using D - K iteration process is designed. Equation (41), as shown at the bottom of the page, describes the robust controller synthesized. For the sake of comparison, the parameters that are employed to synthesize the proposed controller are used in the μ -synthesis-based robust controller (41).

Fig. 3 shows the Test Case I results of the μ -synthesis-based robust controller. Although (41) has been synthesized by a robust control design approach, the controller is unable to catch up with the reference because the controller has been designed for a group of transfer functions to induce robust performance. Therefore, while an optimization process is involved in synthesizing (41), it is not able to perform optimally. The reasoning behind this observation is that the proposed controller has been equipped with a learning mechanism—ensuring optimal performance of the closed-loop system; the μ -synthesis-based robust controller and many advanced classical control techniques do not benefit from such a capability and feature.

For Test Case II, Fig. 4 shows that the proposed controller preserves the synchronization during transients. This matter is critical in low-inertia grids where the synchronization gets lost due to the variations caused by less inertia constant. In contrast, as justified above, the μ -synthesis-based robust controller is unable to do so when the PCC voltage is distorted. Fig. 5 shows the reference tracking capability of the proposed and μ -synthesis-based robust controllers for Test Case III; likewise, the results of the proposed controller outweigh those of the μ -synthesis-based robust controller with the same reasoning stated above.

In order to evaluate the proposed controller and test its learning capability further, Test Case I is repeated for the case where the μ -synthesis-based robust controller is designed for the nominal SCCR of 2 (i.e., weak grid [14]) with the uncertainty range of $1.5 \leq \text{SCCR} \leq 2.5$ to be able to preserve “robust performance.” Still, the grid may get weaker—which is very common in practical systems—so SCCR is equal to 1 (i.e., very weak grid [14]). The proposed controller responds to that change, as depicted in Fig. 3. However, the μ -synthesis-based robust controller causes the

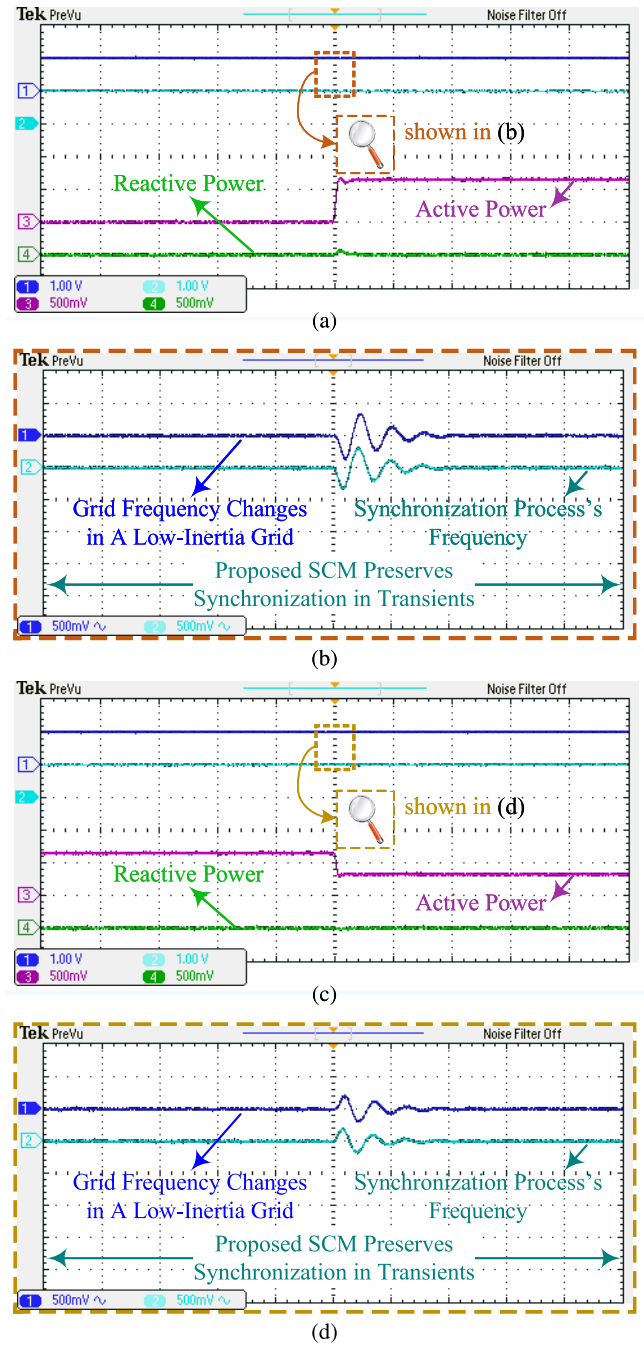


Fig. 10. Experimental results associated with active power changes for the test case employed in simulations: (a) increase in active power showing grid frequency, synchronization process's frequency, active power, and reactive power have been shown by traces in blue, cyan, magenta, and lawn green, respectively, with 60 Hz/div, 60 Hz/div, 3.75 kW/div, and 3.75 kvar/div all with the horizontal axis of 0.5 s/div; (b) the ac components of the frequency signals depicted in Fig. 10a with 0.3 Hz/div with the horizontal axis of 400 ms/div; (c) decrease in active with the signal information detailed in Fig. 10(a); and (d) the ac components of the frequency signals depicted in Fig. 10c with the signal information detailed in Fig. 10(b).

$$K_\mu(s) = \frac{2.203 \times 10^{-5} s^6 + 2.907 s^5 + 2.645 \times 10^7 s^4 + 2.757 \times 10^7 s^3 + 6.195 \times 10^6 s^2 + 2.847 \times 10^5 s + 3646}{s^6 + 1.211 \times 10^4 s^5 + 1.225 \times 10^7 s^4 + 1.392 \times 10^7 s^3 + 5.09 \times 10^6 s^2 + 6.755 \times 10^5 s + 2.158 \times 10^4} \quad (41)$$

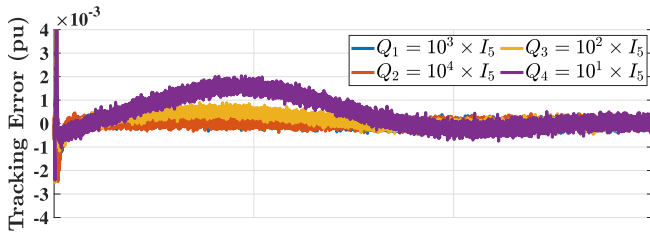


Fig. 11. Experimental results of the performance evaluation of the proposed controller, where I_5 is a 5×5 unity matrix, with the vertical axis of 0.001 pu/div and the horizontal axis of 5 ms/div.

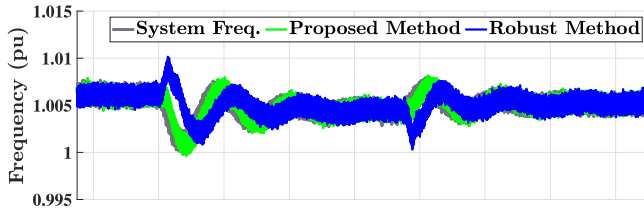


Fig. 12. Experimental results of both proposed and robust methods with the horizontal axis of 200 ms/div.

closed-loop system to get unstable since the controller is unable to self-tune itself, as shown in Fig. 8.

D. Experimental Results of the Proposed Approach

The test rig depicted in Fig. 9 has been used in order to conduct experimental examinations. It is built by the SEMIKRON “SKM 50 GB 123 D” insulated-gate bipolar transistor power modules. Besides, the SEMIKRON “SKHI 21A (R)” gate drives and protection circuitry are employed to make the converter functional. The Verivolt “IsoBlock I-ST-1c”/“IsoBlock V-1c” current/voltage sensors are hooked to digital inputs to measure the current and voltage signals, respectively. The dSPACE “MicroLabBox (MLBX)” real-time digital controller, which also utilizes field-programmable gate arrays, connects the grid-connected IBR under test to the measurement and drive circuits.

Furthermore, effectively controlling the PCC grid is necessary to create a low-inertia and very weak grid with unbalanced voltages to conduct experiments accurately. In this regard, linear power amplifiers from Spitzenberger & Spies are utilized in the test rig. It consists of three linear power amplifiers of 4-quadrant APS 2500 to make a 7.50-kVA, three-phase grid as PCC. The power amplifiers deployed have the characteristics and specifications elaborated in [51]. All of the parameters of the setup deployed are similar to those of simulations, as stated in Table I. Therefore, the comparison between simulation and experiment results is feasible.

Fig. 10 shows the experimental outcomes from the proposed method. Simulations and experiments match well with each other. In this regard, Fig. 10 corresponds with Fig. 3. The consistent agreement between simulations and experimental results reveals the effectiveness of the proposed control for the grid-connected IBR’s synchronization. Fig. 11 evaluates the performance of the proposed controller, and Fig. 12 compares the proposed controller with the μ -synthesis-based robust controller detailed in Subsection IV-C. The

former agrees with the simulations shown in Fig. 6, and the latter agrees with the simulations depicted in Fig. 3, thus demonstrating the superiority of the proposed ADP-based controller.

V. CONCLUSION

Many modern microgrids with a high penetration of power electronic systems and inverter-based resources (IBRs) are utilizing synchronization controls through a synchronization process. However, designing a synchronization control method (SCM) for IBRs in these microgrids has proven challenging due to integrating power electronic converters into unbalanced, low-inertia, and very weak grids. An SCM is unable to respond to all conditions optimally, but an optimal SCM can be designed for a specific grid condition and a particular operating point. This consideration necessitates synthesizing the IBR’s SCM that are able to learn independently, as they are always in demand in the dynamic system’s control design. This paper has proposed an ADP-based method for this problem. To this end, it has first investigated the detailed dynamics of the IBR’s conventional SCM. Afterward, this research has designed an ADP-based optimal controller for the IBR’s SCM. The proposed method has used a data-driven, practical, adaptive, and optimal approach, thus utilizing measurement feedback to control the uncertain dynamics of the synchronization process by the internal model principle. The proposed SCM synthesis has been equipped with an ADP learning methodology based on reinforcement learning to address uncertain parameters and unknown disturbance signals. For comparison, the results of the robust controller designed by the well-established μ synthesis and D - K iteration process have been reported. Simulations, comparative results, and experiments have all revealed the effectiveness and practicability of this research’s ADP-based approach.

REFERENCES

- [1] A. Afshari, M. Davari, M. Karrari, W. Gao, and F. Blaabjerg, “A multivariable, adaptive, robust, primary control enforcing predetermined dynamics of interest in islanded microgrids based on grid-forming inverter-based resources,” *IEEE Trans. Autom. Sci. Eng.*, early access, May 4, 2023, doi: [10.1109/TASE.2023.3262852](https://doi.org/10.1109/TASE.2023.3262852).
- [2] M. Davari, W. Gao, Z.-P. Jiang, and F. L. Lewis, “An optimal primary frequency control based on adaptive dynamic programming for islanded modernized microgrids,” *IEEE Trans. Autom. Sci. Eng.*, vol. 18, no. 3, pp. 1109–1121, Jul. 2021.
- [3] J. Hu, Q. Sun, R. Wang, and Y. Wang, “An improved privacy-preserving consensus strategy for AC microgrids based on output mask approach and node decomposition mechanism,” *IEEE Trans. Autom. Sci. Eng.*, early access, Dec. 22, 2022, doi: [10.1109/TASE.2022.3217677](https://doi.org/10.1109/TASE.2022.3217677).
- [4] K. Liu, F. Gao, Z. Xu, J. Wu, S. Dai, and X. Guan, “Robust constraints-based supply-demand coordination with storage systems of enterprise microgrid,” *IEEE Trans. Autom. Sci. Eng.*, early access, Aug. 24, 2022, doi: [10.1109/TASE.2022.3199776](https://doi.org/10.1109/TASE.2022.3199776).
- [5] Y. Huang, Q. Sun, Y. Li, H. Zhang, and Z. Chen, “Adaptive-discretization based dynamic optimal energy flow for the heat-electricity integrated energy systems with hybrid AC/DC power sources,” *IEEE Trans. Autom. Sci. Eng.*, vol. 20, no. 3, pp. 1864–1875, Jul. 2023.
- [6] C. Zhai, H. D. Nguyen, and X. Zong, “Dynamic security assessment of small-signal stability for power grids using windowed online Gaussian process,” *IEEE Trans. Autom. Sci. Eng.*, vol. 20, no. 2, pp. 1170–1179, Apr. 2023.
- [7] L.-N. Liu and G.-H. Yang, “Distributed fixed-time optimal resource-management for microgrids,” *IEEE Trans. Autom. Sci. Eng.*, vol. 20, no. 1, pp. 404–412, Jan. 2023.

- [8] A. La Bella, S. R. Cominesi, C. Sandroni, and R. Scattolini, "Hierarchical predictive control of microgrids in islanded operation," *IEEE Trans. Autom. Sci. Eng.*, vol. 14, no. 2, pp. 536–546, Apr. 2017.
- [9] D. Wu, T. Yang, A. A. Stoorvogel, and J. Stoustrup, "Distributed optimal coordination for distributed energy resources in power systems," *IEEE Trans. Autom. Sci. Eng.*, vol. 14, no. 2, pp. 414–424, Apr. 2017.
- [10] O. Qasem, M. Davari, W. Gao, D. R. Kirk, and T. Chai, "Hybrid iteration ADP algorithm to solve cooperative, optimal output regulation problem for continuous-time, linear, multi-agent systems: Theory and application in islanded modern microgrids with IBRS," *IEEE Trans. Ind. Electron.*, vol. 71, no. 1, pp. 1–12, Jan. 2023.
- [11] M. Davari and Y. A. I. Mohamed, "Robust DC-link voltage control of a full-scale PMSG wind turbine for effective integration in DC grids," *IEEE Trans. Power Electron.*, vol. 32, no. 5, pp. 4021–4035, May 2017.
- [12] M. Davari and Y. A. I. Mohamed, "Robust droop and DC-bus voltage control for effective stabilization and power sharing in VSC multi-terminal DC grids," *IEEE Trans. Power Electron.*, vol. 33, no. 5, pp. 4373–4395, May 2018.
- [13] P. Mitra, L. Zhang, and L. Harnefors, "Offshore wind integration to a weak grid by VSC-HVDC links using power-synchronization control: A case study," *IEEE Trans. Power Del.*, vol. 29, no. 1, pp. 453–461, Feb. 2014.
- [14] M. Davari and Y. A. I. Mohamed, "Robust vector control of a very weak-grid-connected voltage-source converter considering the phase-locked loop dynamics," *IEEE Trans. Power Electron.*, vol. 32, no. 2, pp. 977–994, Feb. 2017.
- [15] M. Davari, M. P. Aghababa, F. Blaabjerg, and M. Saif, "A modular adaptive robust nonlinear control for resilient integration of VSIs into emerging modernized microgrids," *IEEE J. Emerg. Sel. Topics Power Electron.*, vol. 9, no. 3, pp. 2907–2925, Jun. 2021.
- [16] A. Aghazadeh, M. Davari, H. Nafisi, and F. Blaabjerg, "Grid integration of a dual two-level voltage-source inverter considering grid impedance and phase-locked loop," *IEEE J. Emerg. Sel. Topics Power Electron.*, vol. 9, no. 1, pp. 401–422, Feb. 2021.
- [17] Z. Ali, N. Christofides, L. Hadjidemetriou, E. Kyriakides, Y. Yang, and F. Blaabjerg, "Three-phase phase-locked loop synchronization algorithms for grid-connected renewable energy systems: A review," *Renew. Sustain. Energy Rev.*, vol. 90, pp. 434–452, Jul. 2018.
- [18] K. Givaki, D. Chen, and L. Xu, "Current error based compensations for VSC current control in weak grids for wind farm applications," *IEEE Trans. Sustain. Energy*, vol. 10, no. 1, pp. 26–35, Jan. 2019.
- [19] J. Xu, B. Zhang, Q. Qian, X. Meng, and S. Xie, "Robust control and design based on impedance-based stability criterion for improving stability and harmonics rejection of inverters in weak grid," in *Proc. IEEE Appl. Power Electron. Conf. Expo. (APEC)*, Mar. 2017, pp. 3619–3624.
- [20] S. Zhou et al., "An improved design of current controller for LCL-type grid-connected converter to reduce negative effect of PLL in weak grid," *IEEE J. Emerg. Sel. Topics Power Electron.*, vol. 6, no. 2, pp. 648–663, Jun. 2018.
- [21] D. Zhu, S. Zhou, X. Zou, Y. Kang, and K. Zou, "Small-signal disturbance compensation control for LCL-type grid-connected converter in weak grid," *IEEE Trans. Ind. Appl.*, vol. 56, no. 3, pp. 2852–2861, May/Jun. 2020.
- [22] J. Z. Zhou, H. Ding, S. Fan, Y. Zhang, and A. M. Gole, "Impact of short-circuit ratio and phase-locked-loop parameters on the small-signal behavior of a VSC-HVDC converter," *IEEE Trans. Power Del.*, vol. 29, no. 5, pp. 2287–2296, Oct. 2014.
- [23] Y. Huang, X. Yuan, J. Hu, and P. Zhou, "Modeling of VSC connected to weak grid for stability analysis of DC-link voltage control," *IEEE J. Emerg. Sel. Topics Power Electron.*, vol. 3, no. 4, pp. 1193–1204, Dec. 2015.
- [24] T. Midtsund, J. A. Suul, and T. Undeland, "Evaluation of current controller performance and stability for voltage source converters connected to a weak grid," in *Proc. 2nd Int. Symp. Power Electron. Distrib. Gener. Syst.*, Jun. 2010, pp. 382–388.
- [25] D. Zhu, S. Zhou, X. Zou, and Y. Kang, "Improved design of PLL controller for LCL-type grid-connected converter in weak grid," *IEEE Trans. Power Electron.*, vol. 35, no. 5, pp. 4715–4727, May 2020.
- [26] X. Li and H. Lin, "A design method of phase-locked loop for grid-connected converters considering the influence of current loops in weak grid," *IEEE J. Emerg. Sel. Topics Power Electron.*, vol. 8, no. 3, pp. 2420–2429, Sep. 2020.
- [27] M. Berg, A. Aapro, R. Luhtala, and T. Messo, "Small-signal analysis of photovoltaic inverter with impedance-compensated phase-locked loop in weak grid," *IEEE Trans. Energy Convers.*, vol. 35, no. 1, pp. 347–355, Mar. 2020.
- [28] D. Yang, X. Wang, F. Liu, K. Xin, Y. Liu, and F. Blaabjerg, "Symmetrical PLL for SISO impedance modeling and enhanced stability in weak grids," *IEEE Trans. Power Electron.*, vol. 35, no. 2, pp. 1473–1483, Feb. 2020.
- [29] S. Sahoo, S. Prakash, and S. Mishra, "Power quality improvement of grid-connected DC microgrids using repetitive learning-based PLL under abnormal grid conditions," *IEEE Trans. Ind. Appl.*, vol. 54, no. 1, pp. 82–90, Jan. 2018.
- [30] D. Arricibita, L. Marroyo, and E. L. Barrios, "Simple and robust PLL algorithm for accurate phase tracking under grid disturbances," in *Proc. IEEE 18th Workshop Control Modeling Power Electron. (COMPEL)*, Jul. 2017, pp. 1–6.
- [31] S. Silwal, M. Karimi-Ghartemani, H. Karimi, M. Davari, and S. M. H. Zadeh, "A multivariable controller in synchronous frame integrating phase-locked loop to enhance performance of three-phase grid-connected inverters in weak grids," *IEEE Trans. Power Electron.*, vol. 37, no. 9, pp. 10348–10359, Sep. 2022.
- [32] P. R. Massenio, D. Naso, F. L. Lewis, and A. Davoudi, "Data-driven sparsity-promoting optimal control of power buffers in DC microgrids," *IEEE Trans. Energy Convers.*, vol. 36, no. 3, pp. 1919–1930, Sep. 2021.
- [33] P. R. Massenio, D. Naso, F. L. Lewis, and A. Davoudi, "Assistive power buffer control via adaptive dynamic programming," *IEEE Trans. Energy Convers.*, vol. 35, no. 3, pp. 1534–1546, Sep. 2020.
- [34] W. Gao, Y. Jiang, and M. Davari, "Data-driven cooperative output regulation of multi-agent systems via robust adaptive dynamic programming," *IEEE Trans. Circuits Syst. II, Exp. Briefs*, vol. 66, no. 3, pp. 447–451, Mar. 2019.
- [35] S. Silwal, S. Taghizadeh, M. Karimi-Ghartemani, M. J. Hossain, and M. Davari, "An enhanced control system for single-phase inverters interfaced with weak and distorted grids," *IEEE Trans. Power Electron.*, vol. 34, no. 12, pp. 12538–12551, Dec. 2019.
- [36] T. Chen and B. A. Francis, *Optimal Sampled-Data Control Systems*. Cham, Switzerland: Springer, 1995.
- [37] W. M. Wonham and J. B. Pearson, "Regulation and internal stabilization in linear multivariable systems," *SIAM J. Control*, vol. 12, no. 1, pp. 5–18, Feb. 1974.
- [38] J. Huang, *Nonlinear Output Regulation: Theory and Applications*. Philadelphia, PA, USA: SIAM, 2004.
- [39] C. J. C. H. Watkins and P. Dayan, "Q-learning," *Mach. Learn.*, vol. 8, nos. 3–4, pp. 279–292, 1992.
- [40] Y. Jiang and Z.-P. Jiang, "Computational adaptive optimal control for continuous-time linear systems with completely unknown dynamics," *Automatica*, vol. 48, no. 10, pp. 2699–2704, Oct. 2012.
- [41] F. L. Lewis, D. Vrabie, and K. G. Vamvoudakis, "Reinforcement learning and feedback control: Using natural decision methods to design optimal adaptive controllers," *IEEE Control Syst. Mag.*, vol. 32, no. 6, pp. 76–105, Dec. 2012.
- [42] Y. Yang, K. G. Vamvoudakis, H. Modares, Y. Yin, and D. C. Wunsch, "Safe intermittent reinforcement learning with static and dynamic event generators," *IEEE Trans. Neural Netw. Learn. Syst.*, vol. 31, no. 12, pp. 5441–5455, Dec. 2020.
- [43] P. Lancaster and L. Rodman, *Algebraic Riccati Equations*. New York, NY, USA: Oxford Univ. Press, 1995.
- [44] A. Golieva, "Low short-circuit ratio connection of wind power plants," M.S. thesis, Dept. Electr. Power Eng. Norwegian Univ. Sci. Technol. (NTNU), Trondheim, Norway, Aug. 2015. [Online]. Available: <https://ntnuopen.ntnu.no/ntnu-xmliui/handle/11250/2368039>
- [45] F. D. Freijedo, J. Doval-Gandoy, O. Lopez, and E. Acha, "Tuning of phase-locked loops for power converters under distorted utility conditions," *IEEE Trans. Ind. Appl.*, vol. 45, no. 6, pp. 2039–2047, Nov./Dec. 2009.
- [46] M. Davari, W. Gao, and F. Blaabjerg, "Analysing dynamics and synthesising a robust vector control for the DC-voltage power port based on the modular multilevel converter in multi-infeed AC/DC smart grids," *IET Smart Grid*, vol. 2, no. 4, pp. 645–658, Dec. 2019.

- [47] M. Davari and Y. A.-R.-I. Mohamed, "Dynamics and robust control of a grid-connected VSC in multiterminal DC grids considering the instantaneous power of DC- and AC-side filters and DC grid uncertainty," *IEEE Trans. Power Electron.*, vol. 31, no. 3, pp. 1942–1958, Mar. 2016.
- [48] M. Davari and Y. A.-R.-I. Mohamed, "Robust multi-objective control of VSC-based DC-voltage power port in hybrid AC/DC multi-terminal micro-grids," *IEEE Trans. Smart Grid*, vol. 4, no. 3, pp. 1597–1612, Sep. 2013.
- [49] K. Zhou, J. C. Doyle, and K. Glover, *Robust and Optimal Control*, vol. 40. Upper Saddle River, NJ, USA: Prentice-Hall, 1996.
- [50] G. J. Balas, J. C. Doyle, K. Glover, A. Packard, and R. Smith, *μ -Analysis and Synthesis Toolbox: For Use With MATLAB*. Natick, MA, USA: MathWorks, 1994.
- [51] Spitzberger & Spies. *APS AC/DC 4-Quadrant Voltage Amplifier*. Web Page. Accessed: Nov. 1, 2023. [Online]. Available: <https://www.spitzberger.de/Products-Industry.aspx>



Masoud Davari (Senior Member, IEEE) was born in Isfahan, Iran, in September 1985. He received the B.Sc. degree (summa cum laude) in electrical engineering (power) from the Isfahan University of Technology, Isfahan, in 2007, the M.Sc. degree (summa cum laude) in electrical engineering (power) from the Amirkabir University of Technology (Tehran Polytechnic), Tehran, in 2010, and the Ph.D. degree (Hons.) in electrical engineering (power electronics in energy systems) from the University of Alberta, Edmonton, AB, Canada, in 2016.

He was with the Iran's Grid Secure Operation Research Center and Iran's Electric Power Research Institute (EPRI), Tehran, from January 2010 to December 2011. From April 2015 to June 2017, he was a Senior Research and Development Specialist and a Senior Consultant with Quanta-Technology Company, Markham, ON, Canada, in the field of the dynamic interaction of renewables with smart AC/DC grids and control, protection, and automation of microgrids. In July 2017, he joined as a tenure-track Assistant Professor with the Allen E. Paulson College of Engineering and Computing, Department of Electrical and Computer Engineering, Georgia Southern University (GSU), Statesboro, GA, USA, where he was recommended for being granted early promotion to an Associate Professor and the Award of early tenure in December 2021, and officially approved for both in February 2022. He is the Founder and the Director of the Laboratory for Advanced Power and Energy Systems (LAPES) in the state-of-the-art Center for Engineering and Research established in 2021 with GSU—LAPES can be toured online via the YouTube link (<https://www.youtube.com/watch?v=mhVHp7uMnKo>). He has developed and implemented several experimental test rigs for research universities and the power and energy industry. He has also authored several papers published in IEEE TRANSACTIONS and journals. His research interests include the dynamics, controls, and protections of different power electronic converters utilized in the hybrid AC/DC smart grids and modern power and energy systems testing based on different hardware-in-the-loop (HIL) simulations.

Dr. Davari has been an active member and a Chapter Lead in the IEEE Power & Energy Society Task Force on Innovative Teaching Methods for Modern Power and Energy Systems since July 2020. He has been an active member and a Chapter Lead (for Chapter 3) in the IEEE Working Group P2004—A newly established IEEE working group titled Hardware-in-the-Loop (HIL) Simulation Based Testing of Electric Power Apparatus and Controls for IEEE Standards Association since June 2017. He is an invited member of the Golden Key International Honor Society. He was the Chair of the Literature Review Subgroup of DC@Home Standards for the IEEE Standards Association from April 2014 to October 2015. He is an invited reviewer of several of the IEEE TRANSACTIONS/journals, IET journals, *Energies* journal, and various IEEE conferences, the invited speaker at different universities and in diverse societies, and the Best Reviewer of the IEEE TRANSACTIONS ON POWER SYSTEMS in 2018 and 2020. He was a recipient of the 2019–2020 Allen E. Paulson College of Engineering and Computing (CEC) Faculty Award for Outstanding Scholarly Activity in the Allen E. Paulson CEC at GSU, the Discovery & Innovation Award from the 2020–2021 University Awards of Excellence at GSU, and one of the awardees of the 2021–2022 Impact Area Accelerator Grants (partially funded) at GSU. His biography has been included in *Marquis Who's Who* biographies since 2023. The Awards Committee of the American Society for Engineering Education designated him as the finalist for the 2024 Curtis W. McGraw Research Award in February 2024.



Weinan Gao (Senior Member, IEEE) received the B.Sc. degree in automation and the M.Sc. degree in control theory and control engineering from Northeastern University, Shenyang, China, in 2011 and 2013, respectively, and the Ph.D. degree in electrical engineering from New York University, Brooklyn, NY, USA, in 2017.

He is currently a Professor with the State Key Laboratory of Synthetical Automation for Process Industries, Northeastern University. Previously, he was an Assistant Professor in mechanical and civil engineering with the Florida Institute of Technology, Melbourne, FL, USA, an Assistant Professor in electrical and computer engineering with Georgia Southern University, Statesboro, GA, USA, and a Visiting Professor with the Mitsubishi Electric Research Laboratory (MERL), Cambridge, MA, USA. His research interests include reinforcement learning, adaptive dynamic programming (ADP), optimal control, cooperative adaptive cruise control (CACC), intelligent transportation systems, sampled-data control systems, and output regulation theory. He was a recipient of the Best Paper Award in IEEE International Conference on Real-Time Computing and Robotics (RCAR) in 2018 and the David Goodman Research Award at New York University in 2019. He was a recipient of the U.S.-NSF Engineering Research Initiation Award. He is a member of editorial board of *Neural Computing and Applications* and a Technical Committee Member in IEEE Control Systems Society on Nonlinear Systems and Control and in IFAC TC 1.2 Adaptive and Learning Systems. He was an Associate Editor/a Guest Editor of IEEE/CAA JOURNAL OF AUTOMATICA SINICA, IEEE TRANSACTIONS ON NEURAL NETWORK AND LEARNING SYSTEMS, IEEE TRANSACTIONS ON CIRCUITS AND SYSTEMS II: EXPRESS BRIEFS, *Neurocomputing*, and *Control Engineering Practice*.



Amir Aghazadeh (Graduate Student Member, IEEE) was born in Tehran, Iran. He received the B.S. degree in electrical engineering from the Sadra Institute of Higher Education, Tehran, in 2010, and the M.S. degree in electrical engineering from the Amirkabir University of Technology (AUT), Tehran, in 2014. He is currently pursuing the Ph.D. degree in electrical engineering with the School of Electronic and Electrical Engineering, University of Leeds, Leeds, U.K. He established the Golden Group (G2) at AUT working on emerging and selected topics in

power electronics in 2013. His research interests include power electronics, its application in power systems, and high-speed railway power supply system protection and controls.



Frede Blaabjerg (Fellow, IEEE) received the Ph.D. degree in electrical engineering from Aalborg University, Aalborg, Denmark, in 1995.

From 1987 to 1988, he was with ABBScandia, Randers, Denmark. He became an Assistant Professor, an Associate Professor, and a Full Professor in power electronics and drives with Aalborg University, in 1992, 1996, and 1998, respectively. In 2017, he became a Villum Investigator. Additionally, he was awarded a Honoris Causa from University Politehnica Timisoara (UPT), Timisoara, Romania, and Tallinn Technical University, Tallin, Estonia. He has authored or coauthored four monographs, published more than 600 journal articles in the fields of power electronics and its applications and he was an editor of ten books in power electronics and its applications. His current research interests include power electronics and its applications, such as in wind turbines, PV systems, reliability, harmonics, and adjustable speed drives. He was a recipient of the 33 IEEE Prize Paper Awards, the IEEE PELS Distinguished Service Award in 2009, the EPE-PEMC Council Award in 2010, the IEEE William E. Newell Power Electronics Award 2014, the Villum Kann Rasmussen Research Award 2014, the Global Energy Prize in 2019, and the 2020 IEEE Edison Medal. From 2006 to 2012, he was the Editor-in-Chief of IEEE TRANSACTIONS ON POWER ELECTRONICS. From 2005 to 2007, he was a Distinguished Lecturer of the IEEE Power Electronics Society and the IEEE Industry Applications Society from 2010 to 2011 and from 2017 to 2018. From 2019 to 2020, he was the President of IEEE Power Electronics Society. He was the Vice President of the Danish Academy of Technical Sciences, Lyngby, Denmark. From 2014 to 2020, he was nominated by Thomson Reuters, Toronto, Canada, to be among the most 250 cited researchers in engineering in the world.



Frank L. Lewis (Life Fellow, IEEE) received the bachelor's degree in physics/electrical engineering and the M.S. degree in electrical engineering from Rice University, Houston, TX, USA, in 1971, the M.S. degree in aeronautical engineering from the University of West Florida, Pensacola, FL, USA, in 1977, and the Ph.D. degree in electrical engineering from the Georgia Institute of Technology, Atlanta, GA, USA, in 1981.

He is currently a Distinguished Scholar Professor, a Distinguished Teaching Professor, and the Moncrief-O'Donnell Chair with The University of Texas at Arlington Research Institute, Fort Worth, TX, USA. He has authored seven U.S. patents, numerous journal special issues, journal articles, and 20 books, including *Optimal Control*, *Aircraft Control*, *Optimal Estimation*, and *Robot Manipulator Control*, which are used as university textbooks worldwide. His research interests include feedback control, intelligent systems, cooperative control systems, and nonlinear systems.

Dr. Lewis is a member of the National Academy of Inventors and a fellow of the International Federation of Automatic Control (IFAC) and the U.K. Institute of Measurement and Control (InstMC). He is a professional engineer in Texas, and a Chartered Engineer in the U.K. He was a recipient of the Fulbright Research Award, the National Science Foundation Research Initiation Grant, the ASEE Terman Award, the International Neural Network Society Gabor Award, the U.K. Institute of Measurement and Control Honeywell Field Engineering Medal, the IEEE Computational Intelligence Society Neural Networks Pioneer Award, and the AIAA Intelligent Systems Award. He received the Outstanding Service Award from the Dallas IEEE Section and selected as an Engineer of the year by the IEEE Fort Worth Section. He was listed in Fort Worth Business Press Top 200 Leaders in Manufacturing. He was also a recipient of the Texas Regents Outstanding Teaching Award 2013. He is the founding member of the Board of Governors of the Mediterranean Control Association.